Materials Advances

Accepted Manuscript

This article can be cited before page numbers have been issued, to do this please use: P. Bika, N. Todorova, T. Lymperopoulou, L. Tsakanika, M. A. Gatou, E. Sakellis, N. Zachaopoulos, V. Psycharis, A. Kalafatis, T. Stergiopoulos, D. Tsoukleris, E. Pavlatou and P. Dallas, *Mater. Adv.*, 2026, DOI: 10.1039/D6MA00413J.

View Article Online
DOI: 10.1039/D6MA00413J

Dissolved Oil and Mercury (II) Adsorption under Dynamic Conditions by Thiol-Terminated COF Modified Sponges

Panagiota Bika[a], Nadia Todorova[a], Theopisti Lymperopoulou[b], Lamprini-Areti Tsakanika[b], Maria-Anna Gatou[b], Elias Sakellis[a,c], Nikolaos Zacharopoulos[a], Vasileios Psycharis[a], Apostolos Kalafatis[a], Thomas Stergiopoulos[a], Dimitrios Tsoukleris[d], Evangelia A. Pavlatou[b] and Panagiotis Dallas[a,e]

[a] *Institute of Nanoscience and Nanotechnology, NCSR Demokritos, 15341, Athens, Greece,* [b] *Laboratory of General Chemistry, School of Chemical Engineering, National Technical University of Athens, Zografou Campus, 15772, Athens, Greece* [c] *Department of Physics, National and Kapodistrian University of Athens, Athens, Greece,* [d] *NanoViis Innovative Nanotechnologies 21 El. Venizelou Str., Melissia, Athens, Greece, 15127* [e] *Theoretical and Physical Chemistry Institute, National Hellenic Research Foundation, 11635, Athens, Greece*

- *pdallas@eie.gr; p.dallas@inn.demokritos.gr Phone: +302107273812*

Highlights. Covalent organic frameworks, melamine sponge, heavy metal adsorption, crude oil, oil-in-water emulsion, mercury removal

Abstract

In this work, a multi-step approach for the fabrication of a unique sponge-based platform with multiple functionalities and applications in water remediation technologies under dynamic conditions is presented. Commercial melamine sponges were rendered hydrophobic through the decoration with a vinyl-terminated silane and subsequently were functionalized in-situ through a two-step process with a thiol-terminated covalent organic framework (COF). The materials were extensively characterized and applied for the removal of dissolved oil in an emulsion and mercury cations under dynamic conditions, namely in batch reactor under constant stirring for the oil adsorption and in flow reactor with constant metal concentration for the Hg adsorption. The chemical and structural stability of the COF networks were evaluated

View Article Online
DOI: 10.1039/D6MA00413J

via FTIR, EDS, and SEM analysis, respectively. The oil removal study on a 100 ppm solution with a volume of 100 ml was evaluated through UV-Vis measurements and demonstrated a first-order kinetic fitted with Elovich model, which provided the initial rate α=0.307 mg cm^{-3} min^{-1} and desorption constant β=0.323 g cm^{-3} for the active sites of the thiol-terminated sponges. The competitiveness of a series of elements against mercury adsorption was examined through dynamic absorption experiments and Inductively Coupled Plasma Optical Emission Spectrometry (ICP-OES). A 96-99 % removal of mercury was observed for 300 minutes of continuous flow of a 10 ppm solution and for a subsequent 90 minutes of bypassing a 100 ppm mercury solution removal percentages of 77-96 % was achieved. The characterization analysis and the environmental remediation studies between the efficiencies of COF-modified sponges without and with the -SH terminal groups revealed the crucial role of the thiol pendant groups for both dissolved oil and mercury removal. The versatility of the functional material allows its dual capacity in heavily polluted aqueous environments.

1. Introduction

The contamination of the aqueous environment with crude oil and heavy metals is an ever-increasing threat due to the lack of effective safety measures in industrial sites and cargo ships. [1-2] Various materials have been proposed for the remediation of aqueous environment and melamine sponges appear as a compelling and versatile platform for such applications. [3] Specifically, sponges have been rendered superhydrophobic for ultra-efficient oil-water separation [4] while their functionalization with COFs and hydrophilic layers [5] has enabled the improvement of oil-water separation/purification. [6-7] Crude oil spills clearly present massive environmental destruction, the oil-in-water emulsions appear as an even greater danger. [8] Groundwater contamination is a significant health threat for the local population, and even residential areas have been exposed to petroleum hydrocarbons pollution. [9]

The increased industrialization is also leading to pollution of aqueous resources with heavy metals such as mercury, lead, copper and zinc. Mercury is one of the most toxic heavy metals, with strict regulations for maximum contaminant levels in both water and soil. Soil can be heavily contaminated with mercury due to industrial activities, with concentrations ranging from less than 1 mg kg^{-1} (background levels) up to approximately 10.000 mg kg^{-1} in some cases. [10] Modified sponges are well established as candidates for the removal of heavy metal ions (Hg^{2+}, Pb^{2+}, As^{3+}, Cd^{2+})

View Article Online
DOI: 10.1039/D6MA00413J

from water. [11] Sponges that were functionalized with biogenic methionine resins have reduced the mercury levels to 1.8-4.4 ppb from 200-400 ppb in only 15 minutes as was outlined in the work by Ali et al. [12] A super-amphiphilic silicon sponge was reported to adsorb a high amount of mercury cation with concentrations at the level of 63 – 6231 ppm. The efficiency of the sponge is related to its porosity and the strong affinity between mercury and sulfur. [13] Furthermore, a polyurethane sponge modified with reduced graphene oxide were suggested for both oil-water separation and the removal of divalent copper from wastewater. [14] This nanocomposite exhibited a ~100% removal within 2 h at divalent copper concentration of 6 ppm. Finally, magnetic nanoparticles embedded in melamine sponges have effectively adsorb Pb^{2+} and Cr^{6+} through electrostatic mechanisms. [15]

Recently, we demonstrated the ultra-efficient removal of copper cations from water by a melamine sponge decorated with a triazine based covalent organic framework (COF) bearing terminal 4,4′-bipyridine units. [16] This work was based on our previous identification of reaction mechanism and coordination in divalent copper absorbed by COFs in their powder form. [17] However, these COFs suffered from small porosity, as evidenced by BET measurements. To that end, the imine-linked COFs appear as optimum systems for heavy metal removal. This subclass of covalent organic frameworks has found applications in gas storage and separation, environmental remediation and catalysis. [18-20] Their organic pendant groups can be further modified with a terminal thiol which presents extraordinary ability for mercury and lead removal. [21] Furthermore, by incorporating vinyl silane groups, superhydrophobic property was endowed in the sponges and they have been presented as an ideal system for crude oil removal [22], substantially changing the initial wetting properties and behavior of the commercial melamine sponges [23].

In this work, we present a facile synthesis of an imine-based COF functionalized on hydrophobic sponges for ultra-efficient removal of heavy metal and oil from water. The in-situ reaction is easily scalable with a straightforward modification of more than two (2) grams of melamine sponges in a single batch. The materials absorb crude oil dissolved in water and demonstrate an extraordinary capacity for selective mercury sorption. The former is evidenced by UV-Visible spectroscopy and the latter by ICP-OES. The crucial role of the terminal thiol group providing the materials with amphiphilic properties for both the oil and heavy metal remediation is investigated. The complete removal of mercury cations and dissolved oil in a short period of time were

View Article Online
DOI: 10.1039/D6MA00413J

explained by a first-order kinetic model of oil removal and an accurate fitting with the Elovich equation.

2. Experimental section

2.1. **Materials**.

The commercial Wevora WR-009 melamine sponge was employed as a substrate. Tetraethylorthosilicate (98%, $Si(OC_2H_5)_4$, TEOS) was purchased from Arcos, and the absolute ethanol (99.8%) from Fischer Thermo. The ammonia solution (25%, NH_4OH) was purchased from Carlo Erba, while triethoxyvinylsilane (97%, $C_8H_{18}O_3Si$, VTES) from Thermo Scientific. 1,3,5-tris(4-aminophenyl) benzene (TAB) 97+% and 2,5-divinylterephthaldehyde (Dva) were purchased from BLDpharm. Tetrahydrofuran, o-dichlorobenzene, were purchased from Sigma Aldrich and the radical initiator dibenzoyl peroxide, 97% (dry wt.), wet with 25% water from Thermo Scientific Chemicals.

2.2. **Synthesis of hydrophobic sponges (Sp_h)**.

The commercial melamine sponges were rendered hydrophobic after a two-step process. Initially, a silica layer was formed after condensation of tetraethyl orthosilicate, and then, a second condensation of vinyltrimethoxysilane took place. The synthesis was accomplished following a previously published procedure based on [24]. The sample is denoted as Sp_h.

2.3. **Coating with an imine covalent organic framework (Sp_h_COF)**.

In a scale up procedure, the precursors, along with the hydrophobic sponge, reacted in-situ [4,8], without the use of a radical initiator. 728 mg of hydrophobic sponge Sp-h is added to 70 mL of o-dichlorobenzene and 70 mL of isopropanol. Then, 1.176 g of TAB (3.346 mmol) is added under continuous argon flow, and the mixture is stirred for 5 minutes at 50 ^oC, prior to the quick injection of 0.945 g Dva (5.075 mmol) and 10 mL of acetic acid in the dispersion. The flask is heated under reflux and argon flow at 100 ^oC for 4 hours. Then, the modified sponges are collected via filtration, washed with isopropanol and dried under air. The obtained sample is denoted as Sp_h_COF. As a control experiment, the same COF was synthesized by the reaction of TAB with Dva based on [21] in the absence of the sponge substrates, and the sample is denoted as Powder_ctrl. A second control experiment was performed where a scaled-down condensation reaction in the presence of melamine sponge was left to proceed for 24 hours in toluene (sample denoted as Sp_ctrl).

View Article Online
DOI: 10.1039/D6MA00413J

2.4. **Functionalization with 1,2-ethanedithiol (Sp_h_COF_SH)**.

The weight of Sp_h_COF was measured at 545 mg, and the modified sponges were dispersed in 52 mL of tetrahydrofuran under argon flow. Then, 2.5 mL of 1,2-ethanedithiol and 52 mg of benzoyl peroxide were added to the suspension. The flask was heated at reflux temperature under argon flow. The final sponges were filtered, washed with isopropanol and acetone, and dried under air. The obtained sample is denoted as Sp_h_COF_SH

2.5. **Oil-in-water emulsion adsorption**.

Initially, a concentrated 1000 mg L^{-1} (ppm) emulsion was prepared by adding the appropriate amount of crude oil to 500 mL of deionized water. The crude oil was slowly added (within 10 min) to the water under mixing, and the system was treated for 40 min at a velocity of 5000 rpm using a high shear emulsifier. Then, 50 mL of the prepared emulsion was diluted with deionized water to 500 mL, and the system was treated for 40 min under the same conditions. Thus, a homogeneous oil-in-water emulsion with a concentration of 100 ppm was obtained which was used for the evaluation of the sponges' activity in diluted oil removal. Then, the sponges were added to the emulsion under constant stirring at room temperature. Aliquots were taken at specific time intervals in order their UV-Vis spectra to be measured. Three cycles of adsorption with a duration of 350 min each were performed. After each cycle, the sponges were washed with acetone and air-dried. Samples are denoted as Sp_COF_nc and Sp_COF_SH_nc, where n=1, 2, 3 represents the number of oil adsorption cycles.

2.6. **Heavy metal absorption.**

Dynamic adsorption experiments were carried out using an experimental setup of two small-scale columns to examine the absorption capacity of the materials. The prepared columns were connected to a two-channel microflow variable-speed peristaltic pump, enabling the simultaneous upward inlet of two solutions into the columns. A single element solution prepared from $Hg(NO_3)_2$ salt and a multielement solution prepared with appropriate dilution of the 100 mg•L^{-1} stock CRM 0D7B (CPA Chem) and addition of Hg at a concentration of 10 ppm, were injected through the columns with an upward flow of 0.35 mL•min^{-1} at ambient temperature. The efficiency is calculated by $(C_0 - C_t)/C_0$. The effluents, collected from the top of the columns, were stored at 4 °C prior to analysis by Inductively Coupled Plasma Optical Emission Spectrometry (ICP-OES) using external calibration method.

View Article Online
DOI: 10.1039/D6MA00413J

3. Characterization techniques

The surface morphologies and the Energy Dispersive X-ray Spectroscopy (EDS) elemental analysis were examined using Scanning Electron Microscopy (SEM) using a JEOL 7401f Field Emission. The crystalline structure was analyzed using the X-ray diffraction (XRD) patterns obtained with a Smart Lab Rigaku Diffractometer (Cu Ka radiation). FTIR spectra were recorded on a Thermo Nicolet iS50 instrument in attenuated total reflection mode from 400 to 4000 cm^{-1}. Diffuse reflectance spectra and the spectra used for the evaluation of the oil absorbance were recorded on an Analytik Jena Specord 210 Plus equipped with an integrating sphere. The mercury uptake was studied on an Optima 7000 DV Perkin Elmer Inductively Coupled Plasma Optical Emission Spectrometry (ICP-OES). The surface wettability was evaluated through an Ossila contact angle goniometer. The crude oil emulsion was prepared using a high shear emulsifier Silverson L5M-a

4. Results and discussion

4.1. Chemical and structural characterization of the materials

In this work, hydrophobic melamine sponges were utilized as platforms for the functionalization of an imine-based covalent organic framework. [21] The melamine sponges were initially rendered hydrophobic, through a procedure that involves two subsequent steps of hydrolysis- condensation of the silicon alkoxides TEOS and VTES. The specific reactions for their transformation to silica networks in acidic and alkaline (in our experiment) conditions is well documented in the literature. The mechanism includes (i) gradual hydrolysis of the ethoxy (-OEt) to hydroxyl (-OH) groups and (ii) condensation of H_2O and C_2H_5OH molecules while formation of Si-O-Si bonds [25, 26]. After this modification, the imine COF efficiently coated the sponges following a modified experimental procedure [4,8], using the platform of hydrophobic sponge, the system precursors and Hac as a catalyst. A post-functionalization procedure with 1,2-ethanedithiol resulted in the decoration of the COF with terminal thiol groups, and it was used as the final material for the oil and metal sorption study. The COFs were synthesized with the already established Schiff base condensation reaction among 1,3,5-tris(4-aminophenyl) benzene (Tab) and 2,5-divinylterephthaldehyde (Dva) [27]. The final step was performed by employing the well-known thiol-ene coupling reaction, using benzoyl peroxide as an environmentally friendly radical initiator, instead of azobisisobutyronitrile (AIBN). The steps leading to the fabrication of the final orange-

View Article Online
DOI: 10.1039/D6MA00413J

brown composite are presented in **Figure 1a**. To demonstrate the importance of this system in real-life applications we focused on synthesizing gram-scale quantities of the materials, and we also summarized the other functional materials using with sponge as a matrix that have been used for water remediation in **Table 1**.

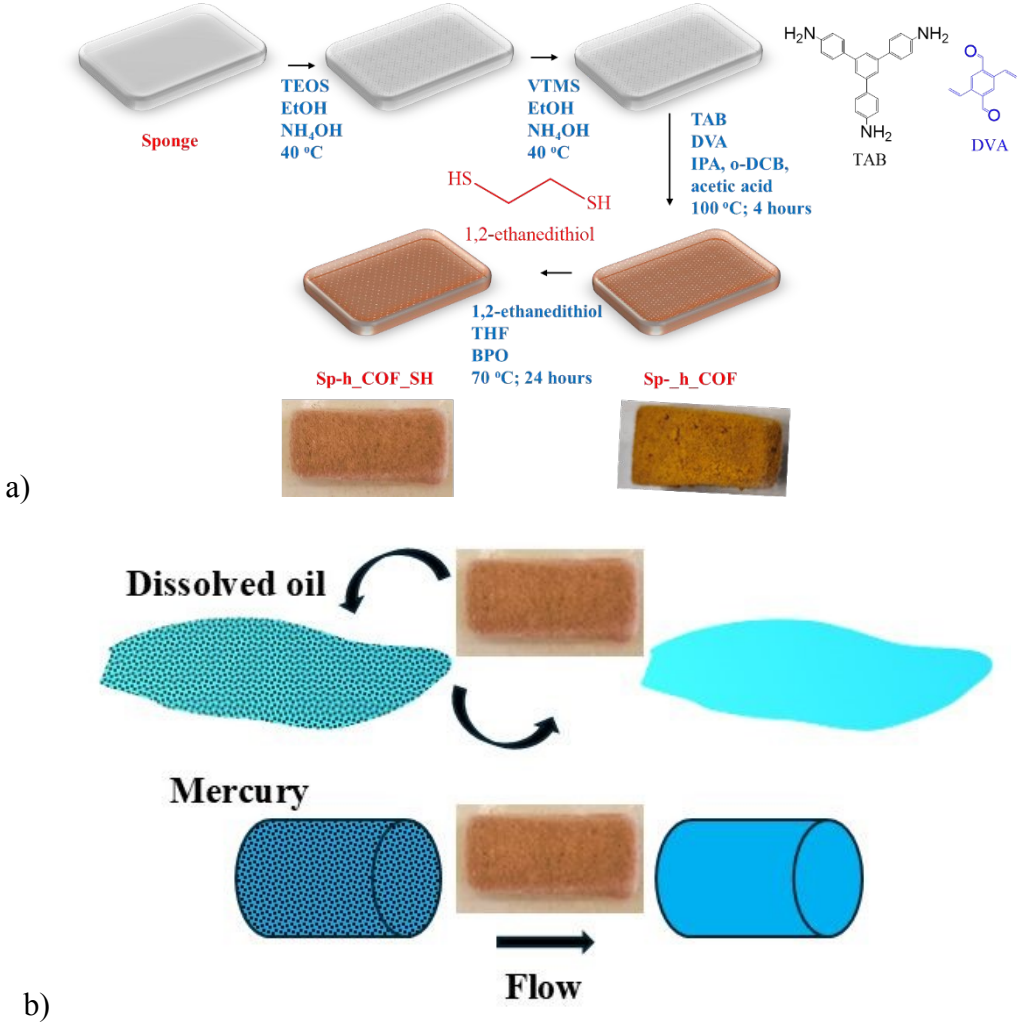

Figure 1. a) Schematic representation of the steps for the fabrication of the thiol (-SH) terminated sponges**,** alongside an image of the modified sponges, b) The two main applications of the sponges: dissolved oil removal under stirring and mercury absorption under continuous flow.

View Article Online
DOI: 10.1039/D6MA00413J

Functional material	Application	Capacity	Reference
Imine COF	Various oils	For silicone oil 150 g g^{-1}, for toluene 125 g g^{-1}	[4]
Organosilane	Various oils	70-120 g g^{-1}	[7]
MnO2/wood	Heavy metals	-	[11]
Silicone sponge	Mercury	941,3 mg g^{-1}	[13]
Reduced graphite oxide	Copper	-	[14]
Triazine COFs	Copper	0.293 mg cm^{-2}	[16]
Magnetic NPs and vinyl terminated silica	Crude oil and heavy metals	60-100 g g^{-1} for crude oil; 20.3-20.5 g g^{-1} for mercury and arsenic	[22]
Vinyl terminated silica	Oil	60-100 g g^{-1}	[24]

Table 1. A summary of sponge-based adsorbers for water remediation technologies.

X-Ray Diffraction was initially employed to prove the formation of covalent organic framework on the surface of the sponges. The two distinctive structures of the COF, before and after the thiol-ene coupling reaction are presented in **Figure 2a**. To obtain a direct comparison with the imine COF, we performed the polycondensation reaction in the absence of sponges, which yielded the pristine powder (Powder_ctrl) and additionally a scaled-down reaction was performed employing a heating time of 24 hours in toluene (Sample: Sp_ctril). The XRD patterns of Sp_h_COF and Sp_h_COF_SH are presented in **Figure 2b,** alongside the diffraction pattern of the control samples and to obtain a direct comparison with the imine COF powder (Powder_ctrl) and sponge (Sp_ctrl). The functionalized sponge Sp_h_COF exhibits the (100) reflection at 2θ=2.73°, which corresponds to the one-dimensional channel with a 32.4 Å diameter [28]. This peak is more pronounced in the two control samples, especially in the Powder_ctrl, due to the hindering effect of the sponges in the formation of a highly ordered, crystalline, framework. In comparison, the Sp_h_COF_SH samples did not demonstrate any pronounced diffraction peaks at low angles, due to a symmetry collapse after the thiol functionalization. The 28.73° peak arises from the melamine sponge. [16]

View Article Online
DOI: 10.1039/D6MA00413J

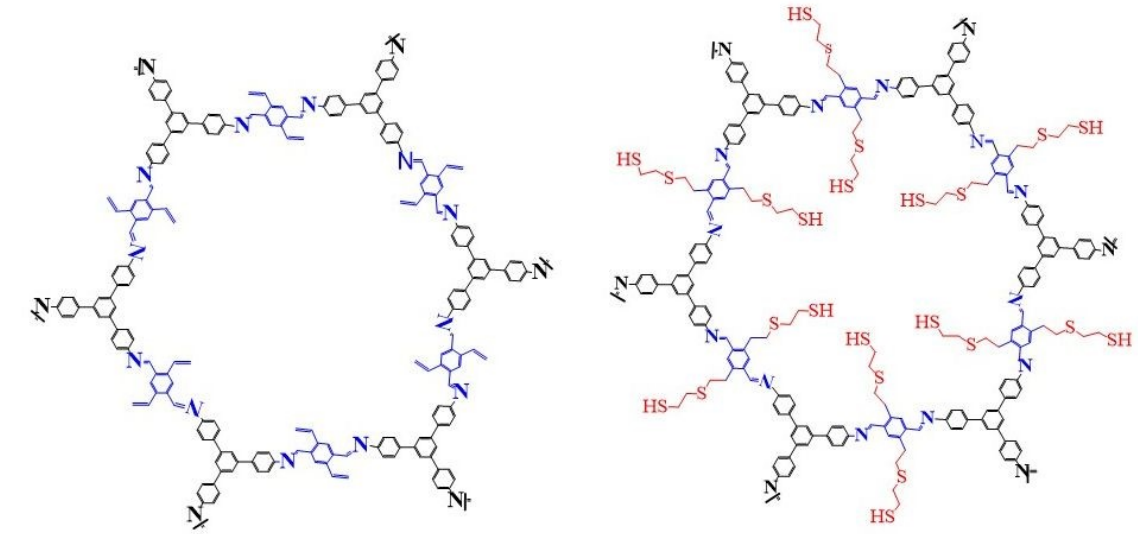

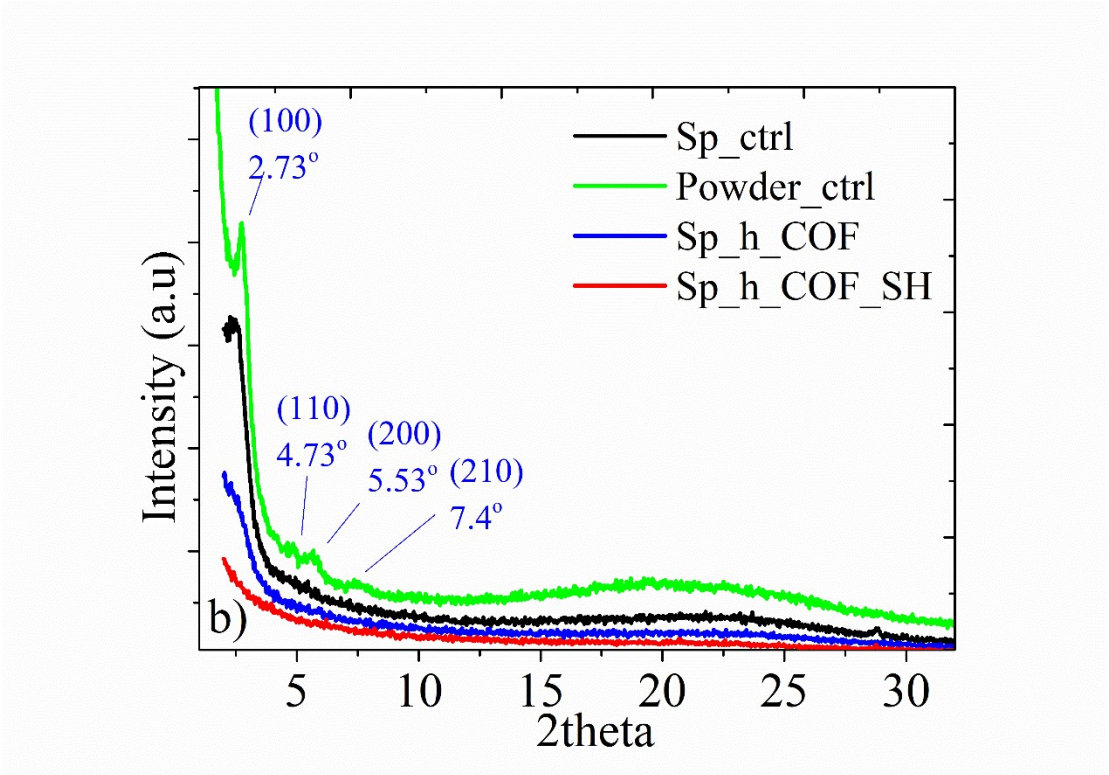

Figure 2. a) The chemical structure of the covalent organic framework with the pendant thiol groups and b) the XRD patterns of the Sp_h_COF, Sp_h_COF_SH and the control samples.

4.2. Evaluation of the stability of the modified sponges during the oil removal process

The sponge-based materials were initially evaluated as adsorbers for crude oil dissolved in deionized water. A representative image of the Sp_h_COF and Sp_h_COF_SH sponges added in the emulsions can be seen in **Figure 3**. The dimensions of the two materials were 1.8•1.2•0.5 cm^3 and 1.4•1•0.5 cm^3 respectively. Before and after the oil removal, a detailed characterization of the materials was conducted to determine their stability and reusability, since both aspects are crucial for real-life applications. As a first step, the density of the materials was calculated. The results are gathered in **Table 2**, where an increase of the sponges' density is observed, after the functionalization reactions. An apparent decrease of density is taking place after the first cycle of the dissolved oil sorption, because of the weakly bound organic moieties' removal during the oil take-up and clean-up procedure with the organic solvents. More specifically, the pristine sponge is an ultra-light, porous material with a density of 8.5 mg cm^{-3}. After its decoration with the hydrophobic silica groups and the covalent organic framework that filled in a large extent the available pores of the melamine substrate, the density was massively increased at 51.5 mg cm^{-3}. Furthermore, the modification with 1,2-ethanedithiol led to a nearly two times increase of the density, which was calculated at 114 mg cm^{-3}. After each oil adsorption and desorption cycle, even if the density decreased due to the removal of the weakly attached organic frameworks, it remained significantly higher than the one of pristine melamine sponge. The density of the COF modified materials is also significantly higher compared to the density that we reported for hydrophobic sponges embedded with iron oxide nanoparticles in our previous work, which was in the level of 10.5-14.2 mg cm^{-3}. [22]

Density (mg cm^{-3})	**Sponge**	**COF functionalized sponge**	**COF-thiol functionalized sponge**
Initial	8.5	51.5	114.0
After cycle No.1	N/A	34.9	37.3
After cycle No.3	N/A	24.8	23.4

Table 2. Density (in mg cm^{-3}) of the pristine sponge and two COF modified samples before and after the oil clean-up process.

View Article Online
DOI: 10.1039/D6MA00413J

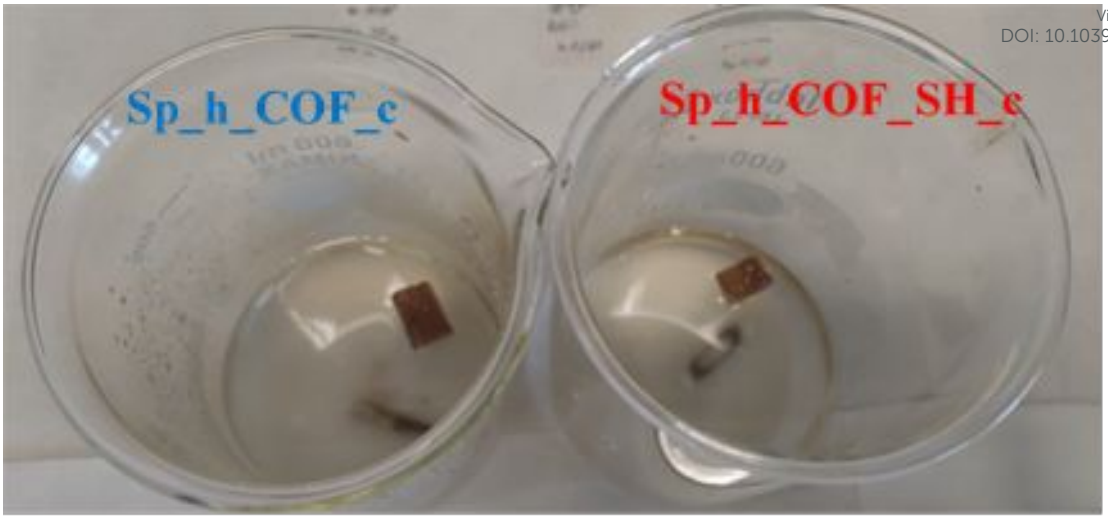

Figure 3. Images of the sponges during the 1st oil adsorption cycle in a batch reactor under constant stirring with a magnet.

The morphology of the modified sponges was evaluated through SEM analysis. The SEM images of the hydrophobic sponge (Sp_h) are published in our previous work [16]. The SEM captures of the Sp_h_COF sample are presented in **Figure 4a** at three different magnifications. The characteristic fibrillar network of the melamine sponge appears covered with the organic framework, while the dense network is forming large agglomerates, intercalated between the fibers of the sponge. After the three cycles of dissolved oil removal and clean-up procedure, it is qualitatively observed that a minor part of the weekly bound physisorbed COFs is removed (**Figure 4b**), and it is additionally explained quantitatively by the decline in density. A similar pattern is observed between the Sp_h_COF_SH and Sp_h_COF_SH_3c samples as well. After the functionalization with the 1,2-ethanedithiol, their morphology remained the same with the network lined up in large aggregates, intercalated between the channels of the melamine sponge (**Figure 4c)**. However, the Sp_h_COF_SH_3c clearly demonstrates a reduced loading of the organic framework agglomerates (**Figure 4d**). This indicates that after the oil adsorption and the subsequent purification process, the thiol-modified frameworks that were physiosorbed on the melamine are removed. These findings coincide well with the calculations performed for the reduced density values, outlined in **Table 2**.

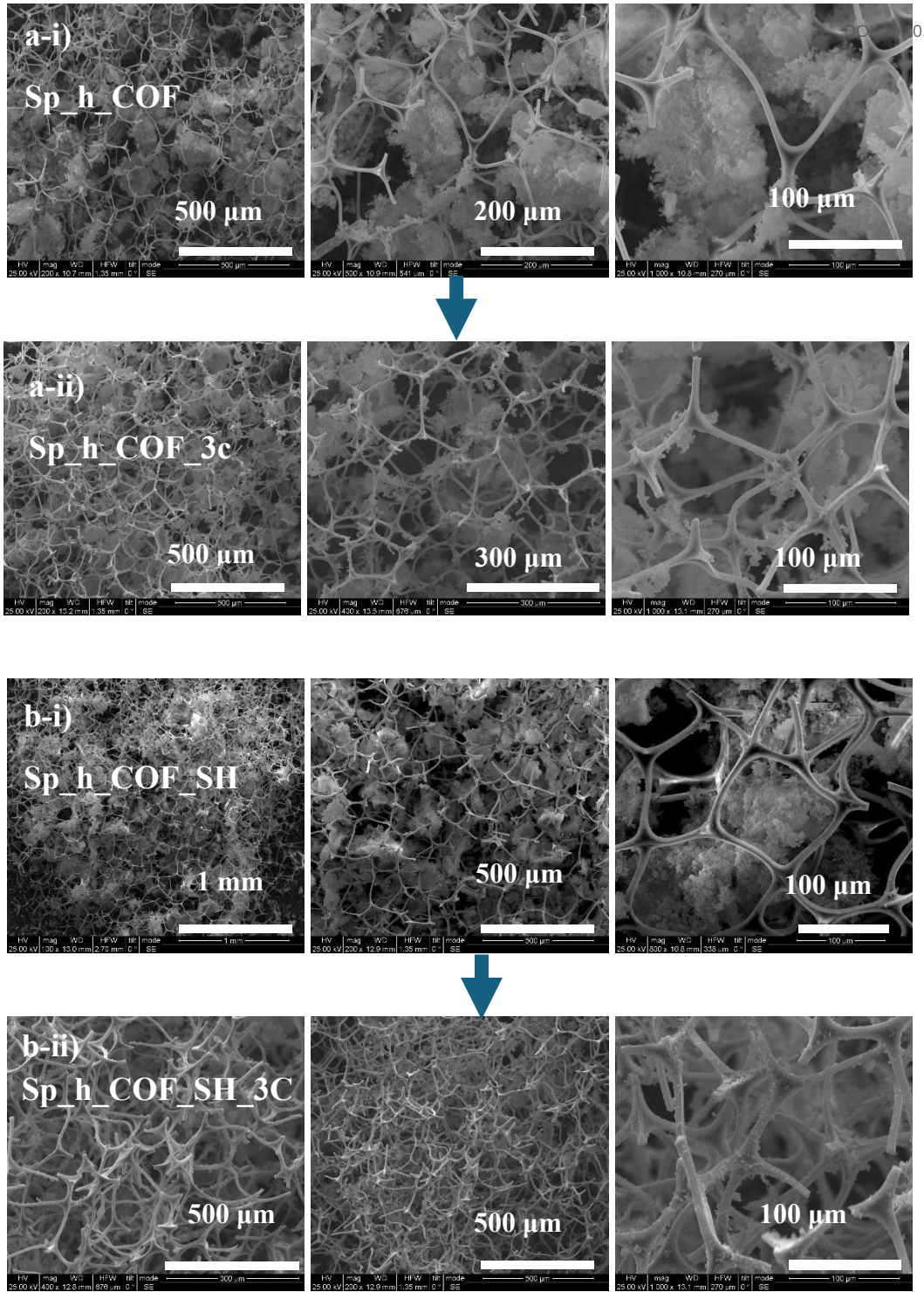

Figure 4. SEM images of a) Sp_h_COF (i) and Sp_h_COF_3c (ii) b) Sp_h_COF_SH (i) Sp_h_COF_SH_3c (ii).

EDS was employed to identify qualitatively and quantitatively the composition of the adsorbers. The focus is shed upon the thiol-terminated sponges before and after the oil adsorption process, since this is the system with the superior performance in the water remediation tests, as it will be discussed in the following sections of the present work.

View Article Online
DOI: 10.1039/D6MA00413J

Representative EDS spectra can be seen in **Figure 5a,** while the atomic and weight percentages derived from two different regions are shown in **Figures 5b-c** and summarized in **Table S1**. The weight and atomic percentages of sulphur are reduced from 14.92 and 6.73 % to 7.88 and 3.34 %, indicating that a fraction of weakly physisorbed COFs is removed during the sorption cycles. However, it unambiguously proves that the thiol groups remain in a reasonably large percentage even after three oil removal cycles, which demonstrates the potential of the material in real life applications.

View Article Online
DOI: 10.1039/D6MA00413J

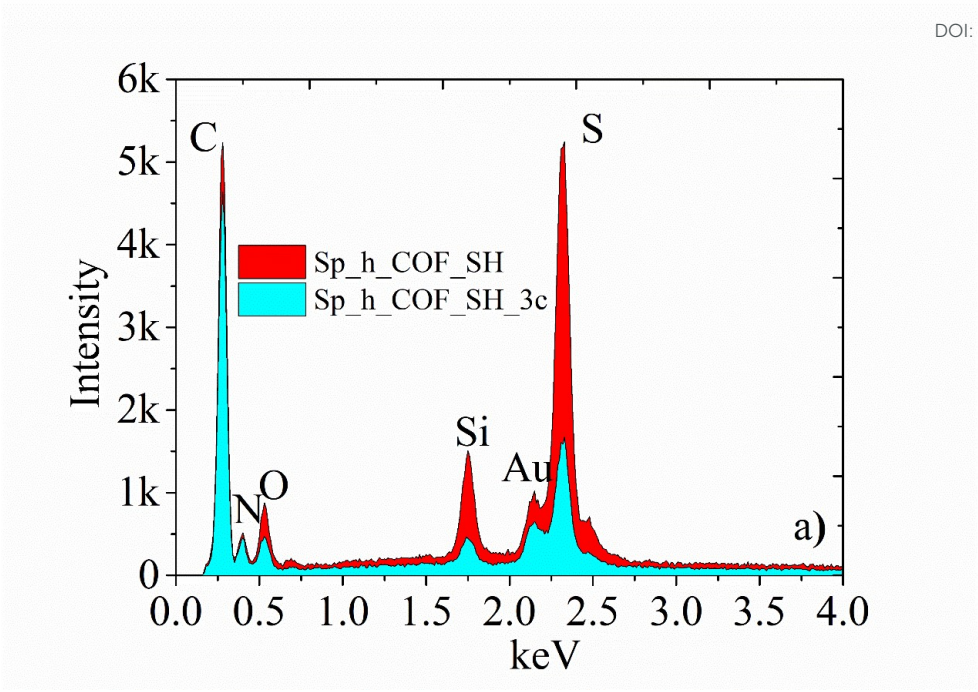

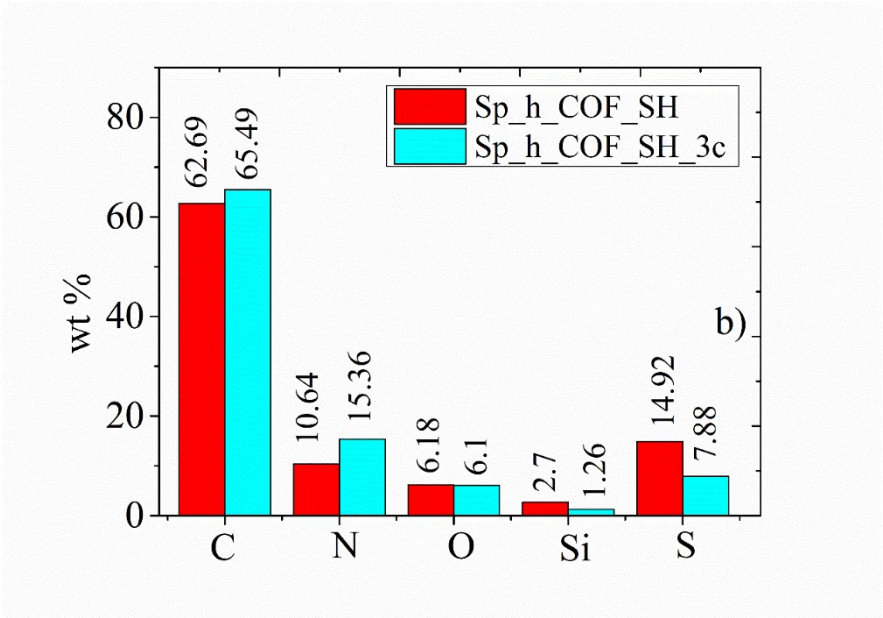

View Article Online
DOI: 10.1039/D6MA00413J

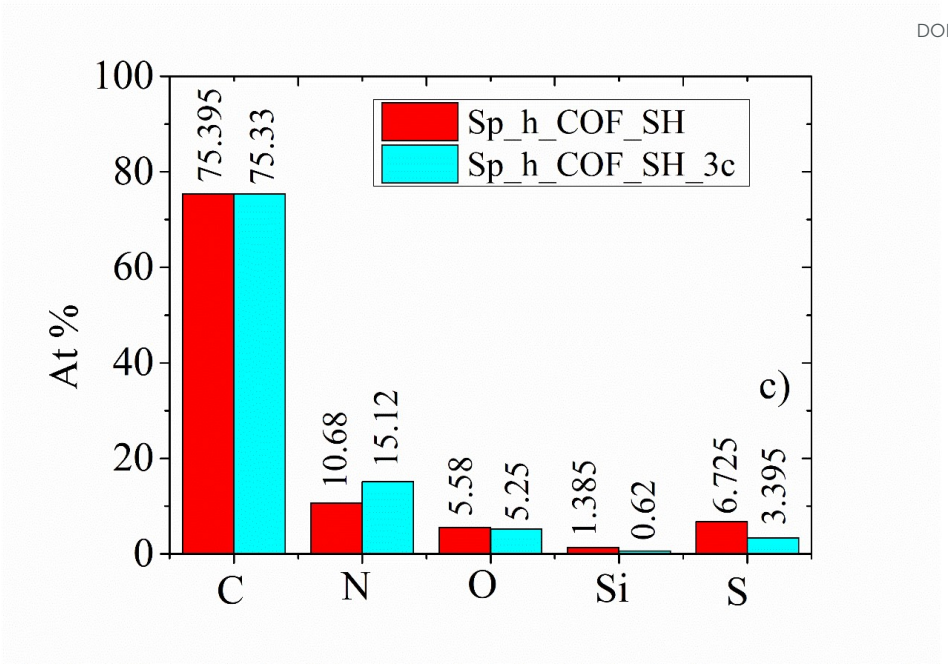

Figure 5. a) Representative EDS spectra for the thiol-modified sponges before (Sp_h_COF_SH) and after 3 cycles of oil removal (Sp_h_COF_SH_3c) and their wt. % (b); at. % (c). The data on (b) and (c) are the average of two different regions.

To further evaluate the influence of the adsorption and desorption oil procedures upon the material, we examined the functionalized sponges through diffuse reflectance and UV-Visible spectroscopy. Their respective diffuse reflectance spectra are demonstrated in **Figure S1** and by considering a direct band gap [29] for the covalent organic frameworks, the Tauc-plots are obtained and presented in **Figure 6a,** along with the derived energy band gaps. The Sp_h_COF exhibits a band gap of 2.38 eV, which remains practically the same after the 3rd cycle of adsorption, with Sp_h_COF_3c at 2.43 eV. An important enhancement of the gap from 2.38 eV of the Sp_h_COF to 2.46 eV with the successful thiol termination in Sp_h_COF_SH is demonstrated due to the presence of non-conjugated aliphatic chains of the thiol. Finally, only a minor increase in the band gap till 2.56 eV is observed for the Sp_h_COF_SH_3c, most likely due to the presence of the non-conjugated oil contaminants. These values greatly match those reported in the literature for imine-linked COFs [30]. A similar increase of the band gap upon methylation of the side chains has been previously observed by Dautzenberg et al. for a series of COFs [30], where their band gaps fluctuated in the range of 2.54-2.93 eV. These observations prove that the COF remains intact during the multi-cycle oil adsorption process.

View Article Online
DOI: 10.1039/D6MA00413J

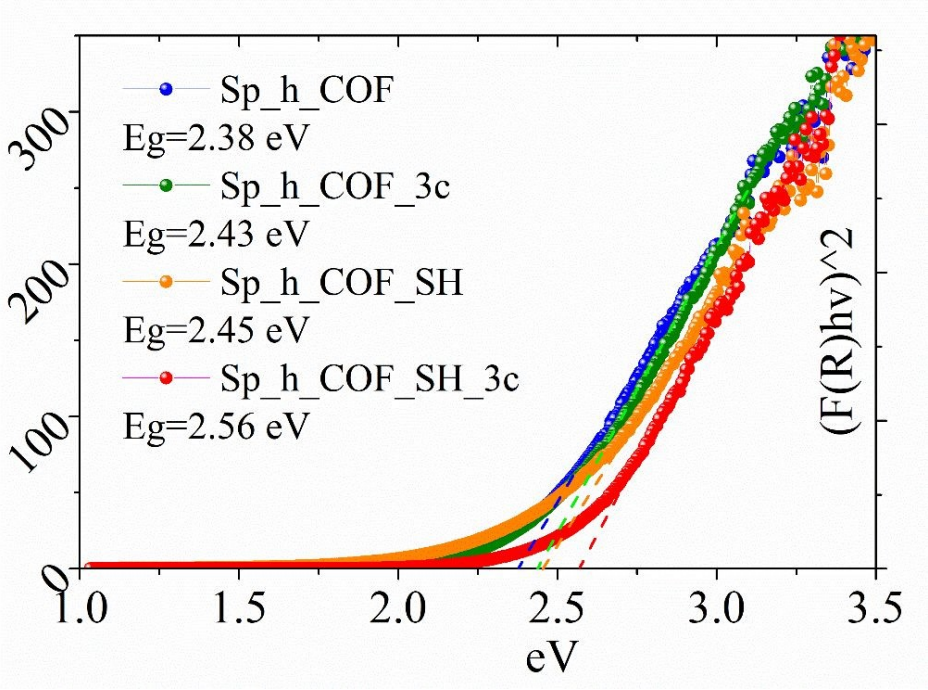

Figure 6. a) Tauc-plots derived from the diffuse reflectance spectra of **Figure S1** for the following samples: Sp_h_COF; Sp_h_COF_3c; Sp_h_COF_SH_3c. The band gaps are indicated in the plot.

The wetting behavior of the functionalized sponges was carefully evaluated through contact angle measurements. Representative images of the three samples with a water drop on their surface can be seen as an inset in **Figure 7**, showing their intense orange-brown color and their texture. In **Figure 7**, the contact angle images are presented for the Sp_COF and Sp_COF_SH samples before and after the first and third cycle of oil adsorption and desorption. The as-made Sp_h_COF and Sp_h_COF_SH samples demonstrate a strikingly different behavior, with the former having a hydrophobic character with a contact angle of 129 °, while the latter has a hydrophilic behavior. However, a superhydrophilic response after a modification with an -SH bond has already been demonstrated in fabrics due to a combination of change of the roughness, van Der Waals forces, and weak hydrogen bonding with water. Li et al compared the wetting behavior of water droplets on a pristine fabric and a thiol-ene/silica hybrid decorated fabric. [31] The water droplets on the pristine fabric had a WCA of 86.4◦, while on the thiol-ene/silica hybrid fabric, water permeated and spread out completely, notably, within 0.36 s. Similarly, in [27] a drastic decline of hydrophobicity was observed, due to changes in the micro- and nano-roughness of their

View Article Online
DOI: 10.1039/D6MA00413J

system. It is known that sulfur has a hydrophobic character, while -SH is more hydrophilic and polar due to its capacity to form H-bonds with water. Depending on the environment, redox conditions can convert the wetting behavior of -S containing groups [32]. Thus, an amphiphilic character, dependent on the surrounding environment and protonation/deprotonation processes (from thiol to thiolate) may be activated. Following the oil adsorption and desorption cycles in this study, the sponges demonstrate hydrophobic behavior, with a contact angle reaching the value of 140.45 ^{o} for the Sp_h_COF_SH_3c sample and 131.60 ^{o} for the Sp_h_COF_3c (**Figure 7c**). In that case, the abundant hydrophobic characteristics of the interior layer in synergy with strongly adsorbed aliphatic or aromatic molecules from the crude oil led to the water-repelling characteristics observed in the water drop experiments. [33] To further evaluate the hydrophobic/hydrophilic properties of the materials, a control experiment was conducted, where the COF powders were removed from the sponges with and without thiol groups, and dispersed them in water. The striking difference between a profound hydrophobic behavior in the powder without the thiol and a stable suspension in the powder with the thiol groups can be seen in **Figure S2**.

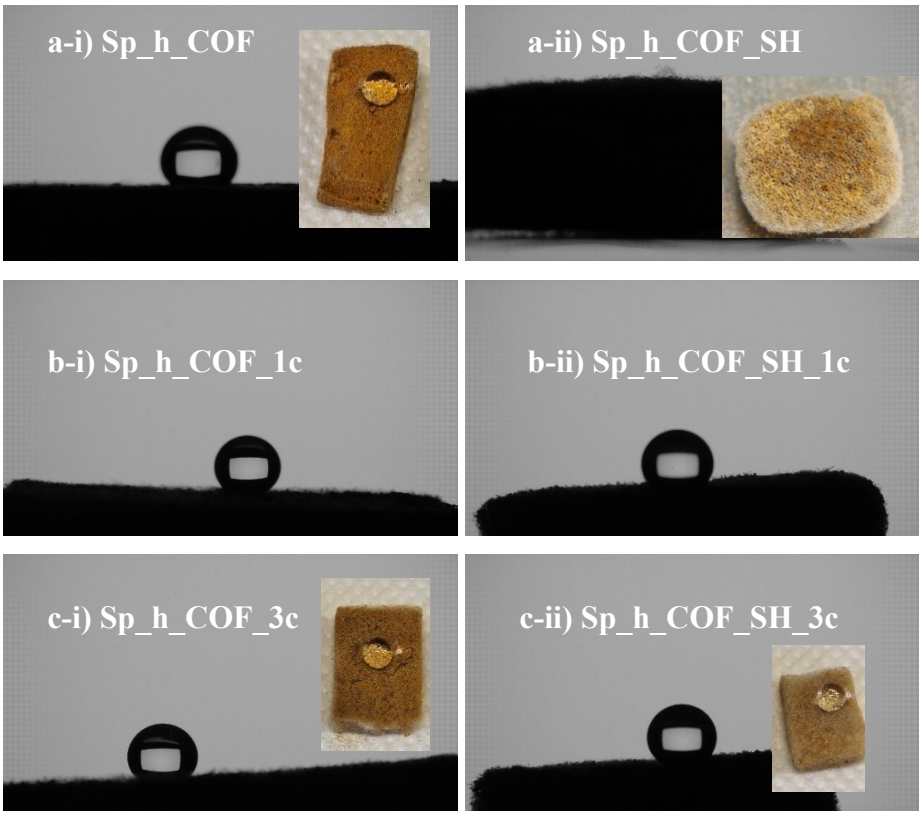

Figure 7. Contact angle measurements for the Sp_h_COF (left) and the Sp_h_COF_SH (right) sponges. a) As-made samples b) After one cycle of oil adsorption-desorption. c)

after three cycles. The images of the sponges with a water drop on their surface appear as an inset.

Vibrational spectroscopy was applied to identify the structure of organic precursor molecules and polymers. The FTIR spectra of the synthesized Sp_h_COF and Sp_h_COF_SH samples before and after oil removal experiments are presented in **Figure S3** to demonstrate the successful synthesis and the chemical stability of the covalent organic frameworks on the hydrophobic sponges and the spectra of the Tab and Dva precursors are presented in **Figure S3c**. In **Figure 8,** the spectra of the COF functionalized sponges, Sp_h_COF; Sp_h_COF_SH; Sp_h_COF_SH_3c are presented alongside the spectrum of the pristine sponge. The COF functionalized sample demonstrates new peaks assigned to the -C=N- and -C=C- double bonds at 1591 and 1517 cm^{-1} [34] and the disappearance of the N-H (peaks at 3432 and 3352 cm^{-1}) related to the Tab as well as the modes at 2700-2780 cm^{-1} characteristic of the aldehyde hydrogen of Dva [4]. The peak at 1683 cm^{-1}, which is characteristic of the aldehyde carbon-oxygen double bond, is also present in the pristine sponge. In Figure S3c we compare the FTIR spectra of the pristine Tab and Dva precursors with the Sp_h_COF sample. While the peak intensity increases in the Sp_h_COF material, which signals some unreacted aldehyde, the rest of the spectrum is markedly different with the precursor molecules. After their functionalization with the dithiol, the vibration peak of the -S-H bond rose in the 2500-2600 cm^{-1} region (**Figure S4**) with a weak intensity. It is important to note that the characteristic peak of the S-H group is notoriously elusive [35] and, in general, exhibits a very low intensity due to the low polarity of the thiol group. In the case of the thiol functionalized sample, after the third oil removal cycle, a significant intensity loss of the characteristic peaks assigned to the COF molecules is observed in the FTIR spectrum, which is in accordance with the fewer population of the agglomerates seen by SEM. The Raman spectra at a green light excitation showed a fluorescence from all samples.

View Article Online
DOI: 10.1039/D6MA00413J

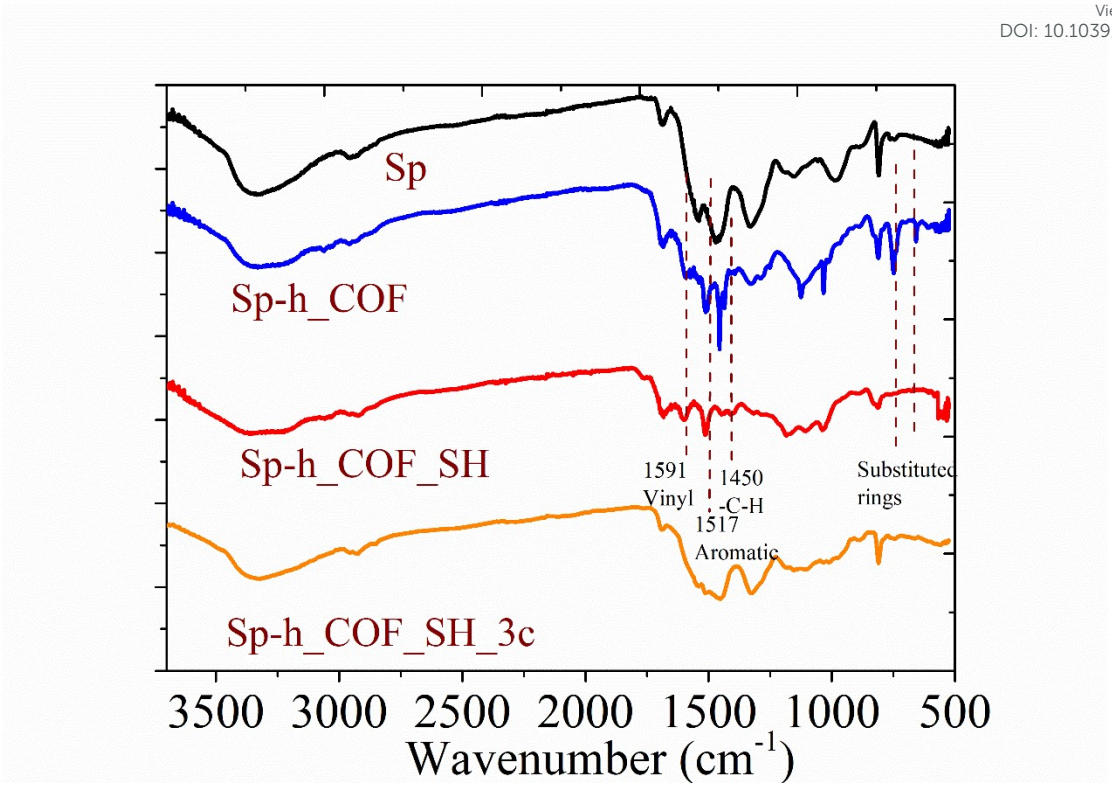

Figure 8. FTIR spectra of Sp, Sp_h_COF, Sp_h_COF_SH and Sp_h_COF_SH_3c.

4.3.The adsorption mechanism of the dissolved oil removal

In this subchapter, a comprehensive study on the kinetic model of the adsorption regarding the dissolved oil and the active sites of the thiol-terminated COF hydrophobic sponges is presented. Our experiment was performed utilizing a stock solution of 100 ppm oil-in-water emulsion, as described in **Section 2.5**. The pH of the emulsion was 6.05. A representative video and image of the preparation of the emulsion can be seen in **Figure S5**. Initially, the absorbance of emulsions ranging from 25 to 2000 ppm of oil was examined to identify the linear region of the absorbance in our spectrometer. The representative graph alongside the image of the dispersions is presented in **Figure S6**. The 100 ppm oil emulsion was kept under vigorous stirring in the presence of the sponge throughout the adsorption experiment. The functionalized sponges were added on the surface of the emulsion and aliquots of 2 mL volume were taken in specific time intervals. The aliquots were returned to the emulsion immediately after recording their UV-Visible spectra. [36] The procedure can be seen in the video of **Figure S7,** where the Sp_h_COF_SH sample is depicted. Finally, the efficiency in oil removal was quantitatively studied using straightforward optical absorption techniques. The adsorption capacity of the sponges was evaluated using the following Equation 1.

View Article Online
DOI: 10.1039/D6MA00413J

$$q_e = \frac{(10 - 10 \bullet \frac{A}{A_0})}{V} \qquad \text{Equation 1}$$

where q_e is the fraction of adsorbed oil from the sponges (mg of oil per cm^3 of sponge; mg cm^{-3}), A is the absorbance measured in different time intervals, A_0 is the absorbance for t=0 min corresponding to 10 mg of oil in the 100 mL of emulsion and V is the volume of the measured sponge.

In **Figure 9a,** the decrease of the A/A_0 with time is presented for the Sp_h_COF and Sp_h_COF_SH samples, while the data regarding the pristine sponge are presented in **Figure S8**. The visible light absorbance was recorded at selected time intervals for a period of 350 minutes, and the final measurement took place after 1440 minutes (24 hours). The Sp_h_COF_SH sample completely removed all the dissolved oil, in contrast to the Sp_h_COF sponge. The quantitative analysis clearly demonstrates the crucial role of the thiol functional group for effective oil adsorption. The pristine sponge absorbs mainly water and minor fractions of oil, while the COF functionalized, hydrophobic sponge, removes oil following a linear decrease of the absorbance value. In contrast, the thiol-modified sponge demonstrates a rapid, exponential decrease of visible light absorbance, related to the oil removal. The Sp_h_COF_SH adsorption curve shown in **Figure 9b** follows a first order kinetic model and the fitting model using **Equation 2**.

$$\ln C_t = -k \bullet t + \ln C_0 \qquad \text{Equation 2}$$

The linear fit with an excellent Adj.R-square=1 results in the following values for the rate constant k=0.01037 min^{-1} and C_0=92.5 ppm. The first-order kinetic model of the process indicates that all adsorption sites have equal energy and chemical properties.

In **Figure 9c,** the adsorption capacity, q_m in mg cm^{-3}, for the Sp_h_COF and Sp_h_COF_SH for three subsequent oil adsorption and desorption cycles is demonstrated. Clearly, the exponential increase of q_m for the thiol-terminated COF is gradually reduced to a linear response after subsequent cycles. At the third cycle, both the pristine and the thiol-terminated samples present an identical behavior, which coincides well with the lesser percent of sulfur as demonstrated by the EDS analysis. In order to explain these results, we take a careful look at the composition of the crude

View Article Online
DOI: 10.1039/D6MA00413J

oil. Crude oil itself contains sulfur, thiols, as well as metals that have a high affinity with the -S-H group. [37-38] Furthermore, the functionalization with 1,2-ethanedithiol inherited the sponges with two additional hydrocarbon groups. Hence, we assign the high efficiency of the Sp_h_COF_SH sample to the combination of the above-mentioned factors.

Additionally, the kinetics of the adsorption were described through a widely used equation, which represents the Elovich model. The equation of the Elovich kinetic model is described by the following equation:

$$q_t = \frac{1}{a}\ln(\alpha \bullet \beta) + \frac{1}{a}\ln(t) \qquad \text{Equation 3}$$

where q_t (mg cm^{-3}) is the adsorption capacity in each time interval, t is the time (min), α is the initial adsorption rate, and β is the desorption constant. The Elovich model describes the adsorption kinetics considering the chemisorption mechanism, where the adsorption rate decreases exponentially as the adsorbed amount increases. It describes activated adsorption, where reaction occurs on localized sites and leads to a decrease in rate as the active sites become occupied. [39] This is assigned to the heterogeneous nature of solid surfaces and the increase in occupied active sites. The obtained parameters of the initial rate α, and desorption constant β, indicate strong attachment and surface irregularities, respectively. The excellent fitting with adj-R square=0.983 indicates a surface with varied active binding sites, where the most efficient sites are filled first, rapidly, slowing and hindering the overall rate (**Figure 9d**). A second order kinetic fitting was also applied and presented a non-linear growth rate (**Figure S9**). [40]

In general, crude oil sorption is a complex process involving physisorption through weak Van Der Waals forces, strong chemical interactions (i.e. chemisorption) through the functional groups of the organic molecules and sulfur and metal components and pore diffusion, with the latter being in general the rate-determining step. [41-42]

The linear fitting using the Elovich model provides the following values: **α=0.307** mg cm^{-3} min^{-1} & **β=0.323** g cm^{-3}. The α parameter represents the initial adsorption rate and indicates how quickly the adsorption process begins, while the β constant is related to the extent of surface coverage and the activation energy for the sorption. [43] Additionally, the data were fitted using the Bangham model, a diffusion

View Article Online
DOI: 10.1039/D6MA00413J

kinetic model of substances within the pores of the adsorbent while a reaction happens at the liquid/solid interface. The Bangham model with an adj-R square=0.9, in **Figure S10,** indicates that the mass transfer is limited and diffusion is not the rate determining step.

View Article Online
DOI: 10.1039/D6MA00413J

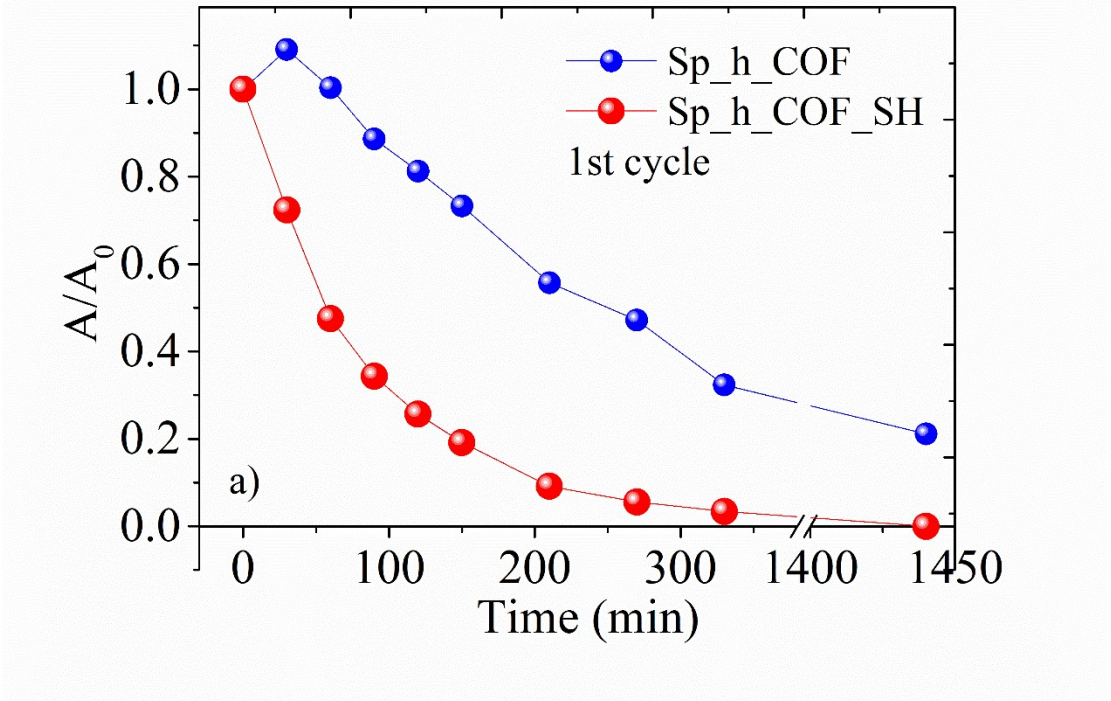

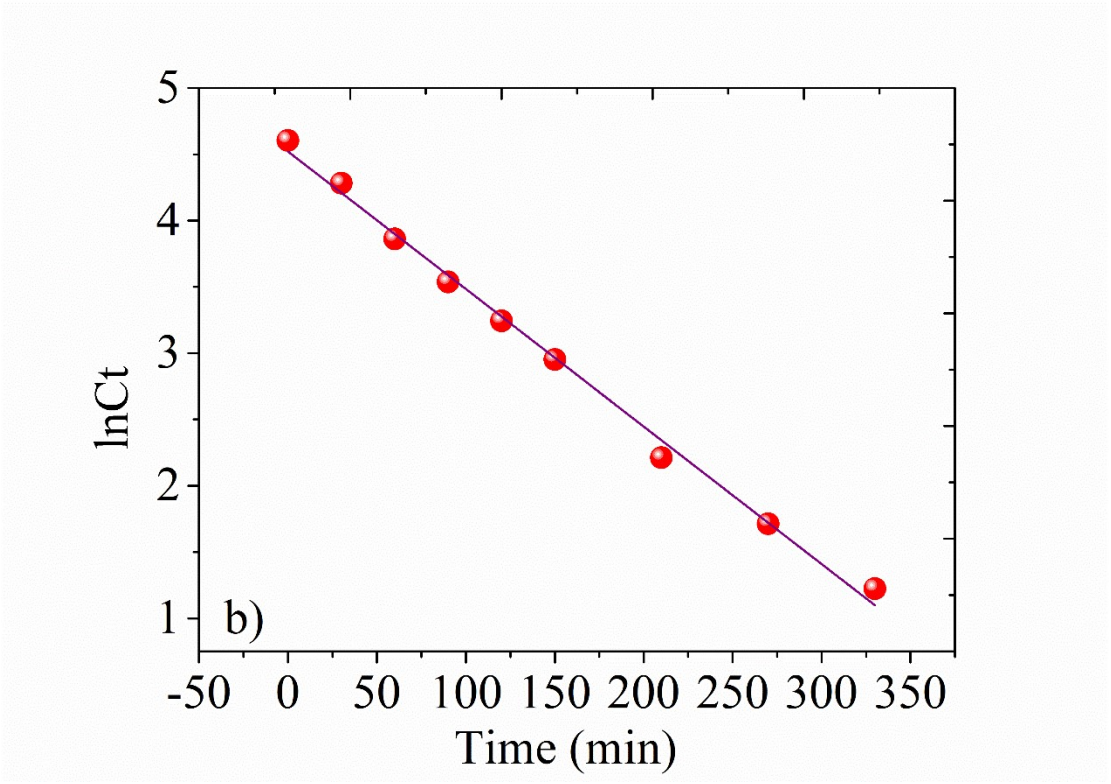

View Article Online
DOI: 10.1039/D6MA00413J

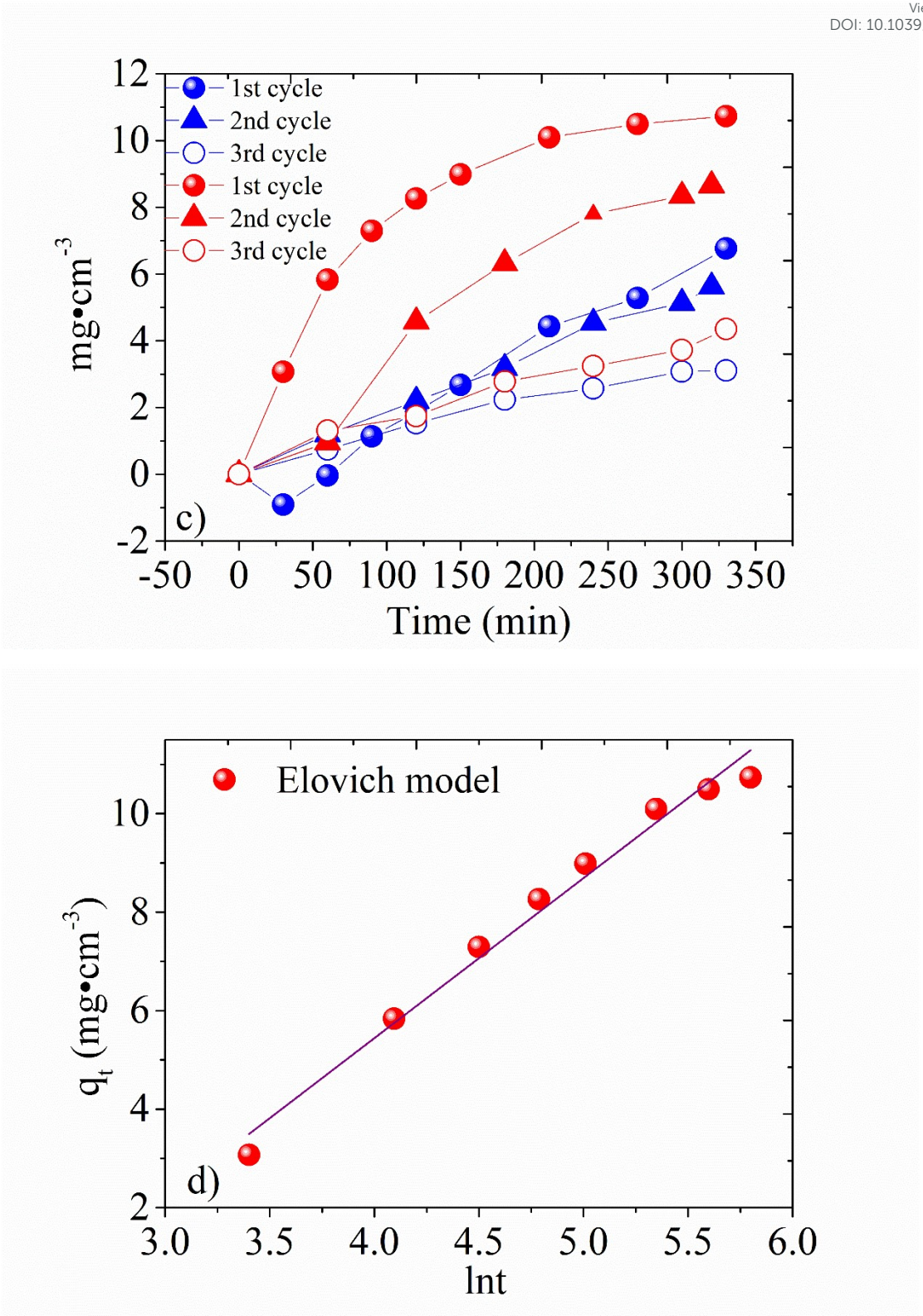

Figure 9. a) The decrease of the oil absorbance at 700 nm (A) with respect to the initial value (A_0) for the two composite sponges, b) First order kinetics fitting for the Sp_h_COF_SH sample, c) Kinetic adsorption graphs for the Sp_h_COF (blue curves) and Sp_h_COF_SH (red curves) for the 1st; 2nd and 3rd run of oil adsorption and

View Article Online
DOI: 10.1039/D6MA00413J

desorption and d) the Elovich fitting model for the Sp_h_COF_SH representing the first oil removal cycle.

4.4.Mercury removal from aqueous solution

The design and synthesis of functional materials with high selectivity and sensitive detection are crucial for contemporary environmental science and its applications. Terminal groups are introduced in porous materials to render them suitable for the chemisorption of metallic cations. Typical characteristic groups that decorate both metal organic and covalent organic frameworks and other porous media include thiol, oxime, and thiourea functional groups, containing S, N, or both N and S elements. These groups enable the ultra-efficient complexation of cations such as Pb^{2+} and Hg^{2+}. For Hg^{2+}, a record-breaking adsorption capacity (957.94 mg g^{-1}, 1.99 times that of unmodified materials) and distribution coefficient (743333 mL g^{-1}) have been observed for functionalized metal organic frameworks such as the well-known MOF 808. [44]

The metals removal capacity of the composite sponges was evaluated under dynamic adsorption experiments, which are considered closer to real-life applications compared to static experiments. As a control experiment, the functionalized sponge with the imine COF was studied initially prior to the thiol modification. These nitrogen-rich COFs have been previously demonstrated to be efficient absorbers for mercury cations. [45] For the experiments of this study, an aqueous solution of mercury nitrate and a multielement standard solution that contains 27 different elements were utilized. The pH of the mercury nitrate and of the multielement solution was 3.5 and 1, respectively. It is considered that the pH greatly influences the mercury behavior and its solubility in water. At very low, acidic pH levels, mercury is predominantly in the form of "free" divalent cations, i.e. Hg^{2+}. As the pH levels increase, the hydroxide $HgOH^-$ form dominates. Thus, the dominant mercury species in the solution are Hg^{2+} at pH<3.0, and $Hg(OH)_2$ at pH>5 and both species alongside $HgOH^+$ co-exist between pH 3 and pH 5. [46-47] This is outlined in the chemical equations that can be seen below.

$Hg^{2+} + OH^- \leftrightarrow HgOH^+$ $K_3=10^{10.6}$ Equation 4

$HgOH^+ + OH^- \leftrightarrow Hg(OH)_2$ $K_4=10^{11.2}$ Equation 5

$Hg(OH)_2 + OH^- \leftrightarrow Hg(OH)_3^-$ $K_5=10^{-0.9}$ Equation 6

In dilute solution, mercury species at different pH values are calculated according to the above equilibrium constants, and are denoted as α'_0, α'_1, α'_2 and α'_3. They represent the percentages of Hg_2^+, $HgOH^+$, $Hg(OH)_2$ and $Hg(OH)_3^-$ respectively following the trend seen in **Figure 10a**.

$$\alpha'_0=1/[K_3\bullet[OH^-]+K_3\bullet K_4\bullet[OH^-]^2+K_3\bullet K_4\bullet K_5\bullet[OH^-]^3 \quad \text{Equation 7}$$

$$\alpha'_1= \alpha'_0\bullet K_3\bullet[OH^-] \quad \text{Equation 8}$$

$$\alpha'_2= \alpha'_0\bullet K_3\bullet K_4\bullet[OH^-]^2 \quad \text{Equation 9}$$

$$\alpha'_3= \alpha'_0\bullet K_3\bullet K_4\bullet K_5\bullet[OH^-]^3 \quad \text{Equation 10}$$

In the experiments, we observed a drastically different behavior of the Sp_h_COF sample, where almost no mercury uptake was observed in the mercury nitrate solution, while a rapid and more efficient removal was achieved at the multielement solution (**Figure 10b**). As the pH of the mercury nitrate solution is 3.5 and of the multielement solution is highly acidic with a pH=1, we assign this discrepancy to the inactivity of the nitrogen moieties to successfully coordinate with $HgOH^+$ in contrast with the divalent cation. The efficiency of the system in sequestering mercury is determined by the delicate balance between metal speciation and the protonation state of the imine linkages. At pH 1, mercury exists primarily as the free mercuric ion Hg^{2+}, which acts as a potent and "soft" Lewis acid. Due to its high polarizability, Hg^{2+} tends to withdraw electron density from the imine N=C bond, even when the nitrogen is already protonated RN=CR-H^+. At pH 1, complete protonation of the imines strongly polarizes the N=C bond, creating an electronic environment conducive to Hg^{2+} entry. The mercury coordinates with nitrogen, while the framework architecture keeps the carbon protected from water-induced hydrolysis. The free, "softer" Hg^{2+} form allows interaction with the double bonds of the COF. These interactions stabilize the metal within the lattice. Conversely, at pH 3.5, the emergence of $[Hg(OH)]^+$ a "harder" Lewis acid, and the lack of full imine protonation limit the binding affinity. [48]

Following the soft and hard acid-base theory, sulfur containing groups are excellent candidates for the removal of mercury from aqueous solutions. Mercury, particularly in forms like Hg^{2+} and methylmercury, is classified as a soft Lewis acid. This large cation with low charge density is highly polarizable. Sulfur-containing compounds such as sulfides (S^{2-}) and thiolates (SH^-), are highly polarizable with low electronegativity, thus

View Article Online
DOI: 10.1039/D6MA00413J

are classified as soft Lewis bases. With respect to the above, mercury has a high affinity for sulfur, leading to the formation of very stable, insoluble complexes. The reaction thermodynamics prove the high affinity of mercury to sulfur (i.e., log K≈52.7–53.3) compared to that for Hg to organic matter (i.e., log K = 22–28). [49] Under the dynamic, continuous flow conditions the Sp_h_COF_SH samples presented a complete removal of mercury for 300 minutes when the solution had a concentration of 10 ppm (**Figure 10c**). We then switched to a 100 ppm solution where a partial saturation of the capacity was observed. The material reached saturation much earlier when a multielement solution was applied (**Figure 10d**) due to competition from other metal cations. Specifically, we identified the removal of lead during the experiments with the multi-element solution. A detailed study focusing on the competition between the different heavy metals, specifically on the Pb^{2+}, would be a subject of a separate work.

In **Figure 10e**, we present the images of the sponges after the dynamic experiments, where it is noteworthy that the Sp_h_COF_SH sample retained its hydrophilicity with the water droplet readily spreading on its surface. The thiol terminated sponges obtained a darker color after the mercury adsorption in both single element and multiAdditionally, EDS analysis proved the presence of both sulfur and mercury, with the characteristic Hg L peaks appearing at high energies, while the Hg M and the S K peaks overlap, as expected (**Figure 10f**). At the inset graph added in **Figure 10f-i,** the deconvolution reveals the two distinctive peaks at 2.2 keV for the Hg and 2.3 keV for the S element. In **Figure 10f-ii** the respective quantitative analysis is demonstrated and reveals an atomic percent of 4.29 % for the sulfur element and 2.36 % for the mercury (see also **Table S2**). The system before Hg(II) adsorption consists of higher percentages in C, N, S elements than after the adsorption experiments, which is a natural consistency with the physisorbed quantities drifted by the flow of the solution. Though the Sp_h_COF_SH contains lower quantity of O and Si in comparison to the aftermath values of the dynamic adsorption experiment. Si values may be increased due to the reveal of the hydrophobic layer from the physisorbed molecules carried away, and O has its source from the $Hg(NO_3)_2$ aqueous solution. The SEM images of the three systems after the heavy metal removal application are presented in **Figure 11**. It appears that the materials remained practically the same, which further strengthens their positive aspects for everyday and industrial applications. The Sp_h_COF_SH after mercury adsorption (**Figure 11b**) presents a more continuous bonded network in comparison to the initial agglomerates.

View Article Online
DOI: 10.1039/D6MA00413J

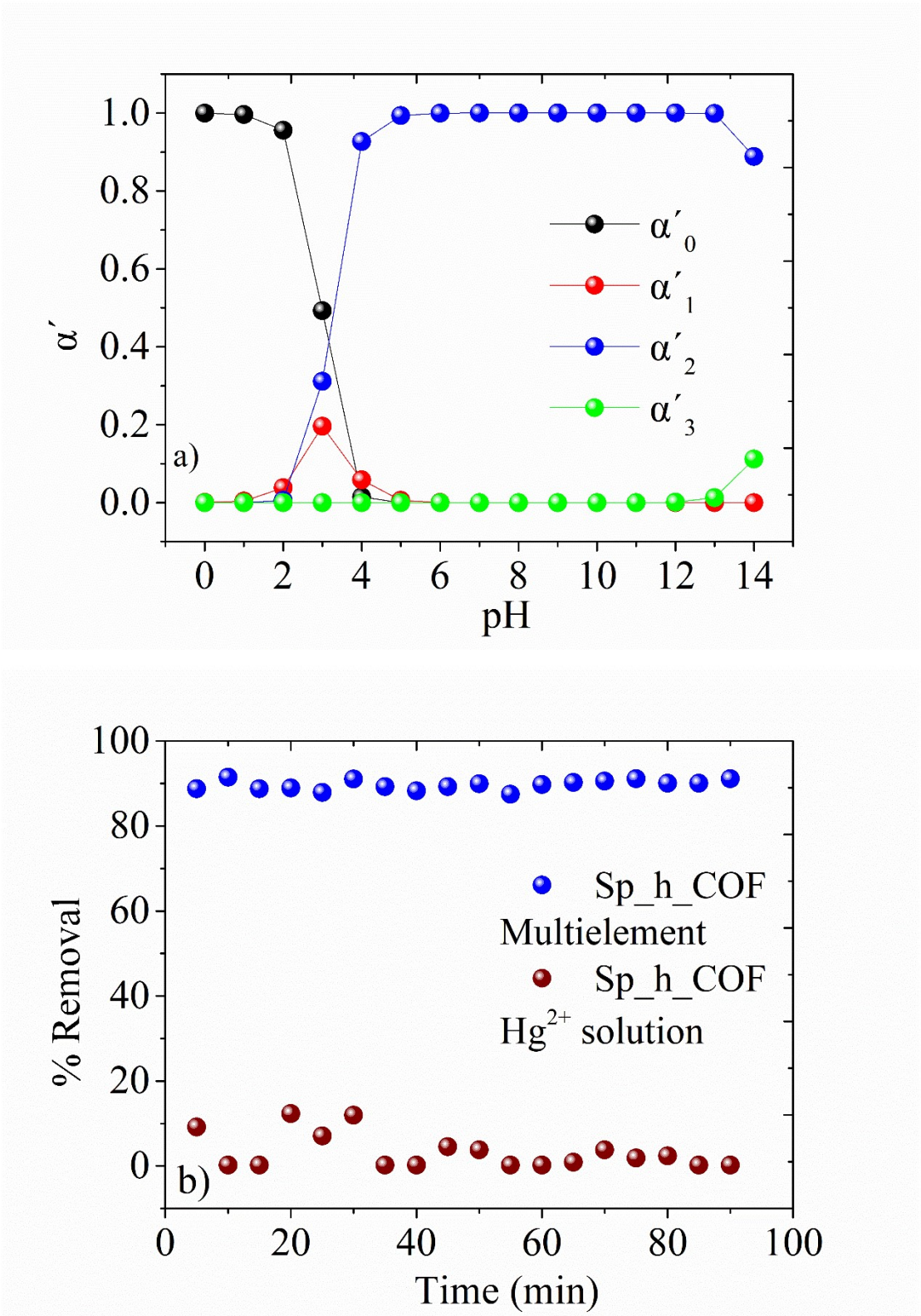

View Article Online
DOI: 10.1039/D6MA00413J

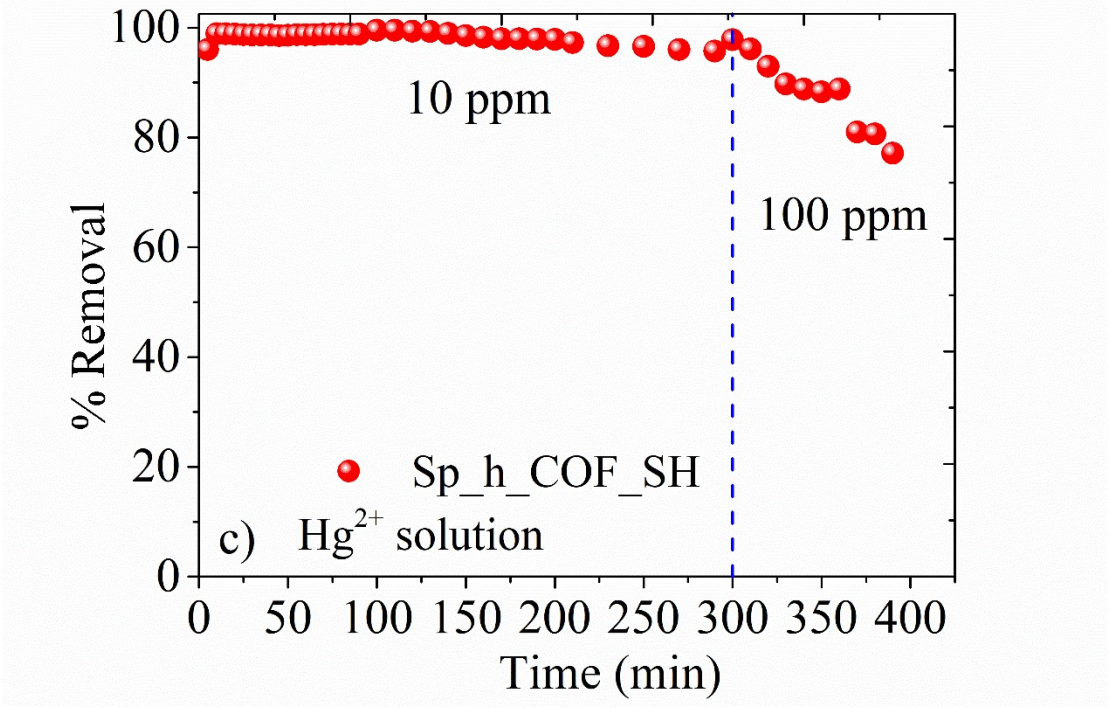

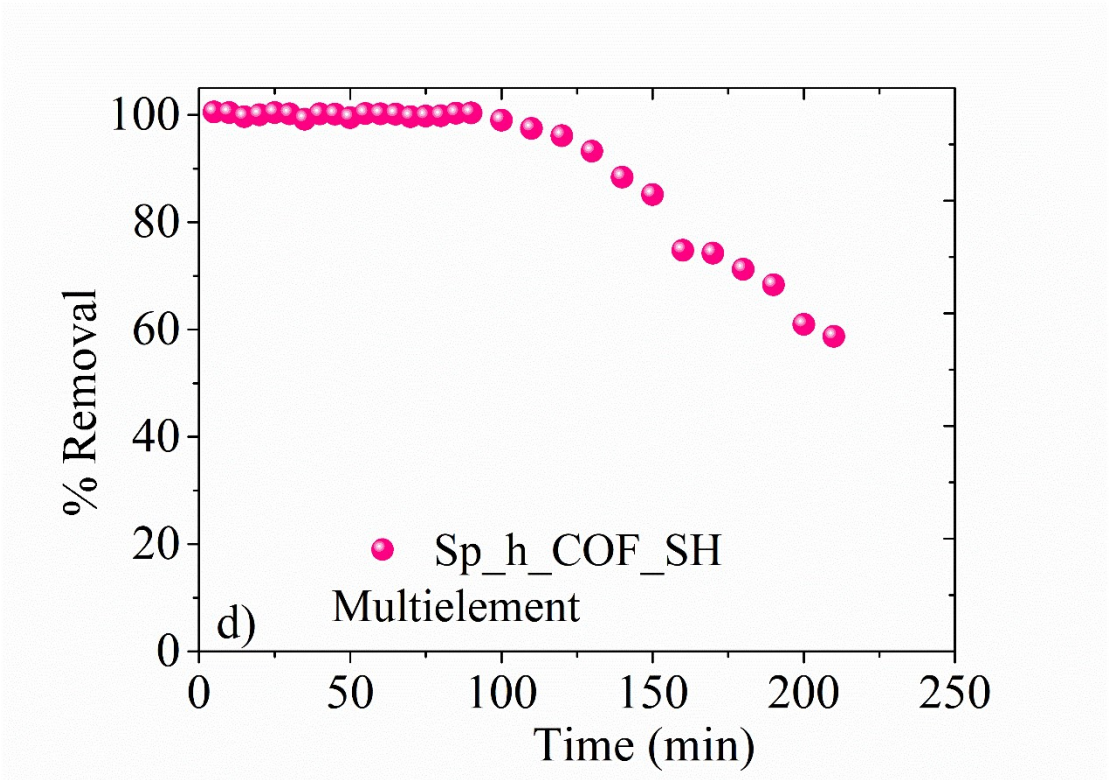

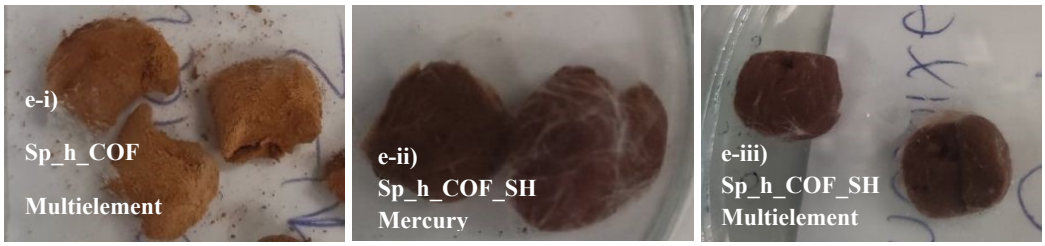

View Article Online
DOI: 10.1039/D6MA00413J

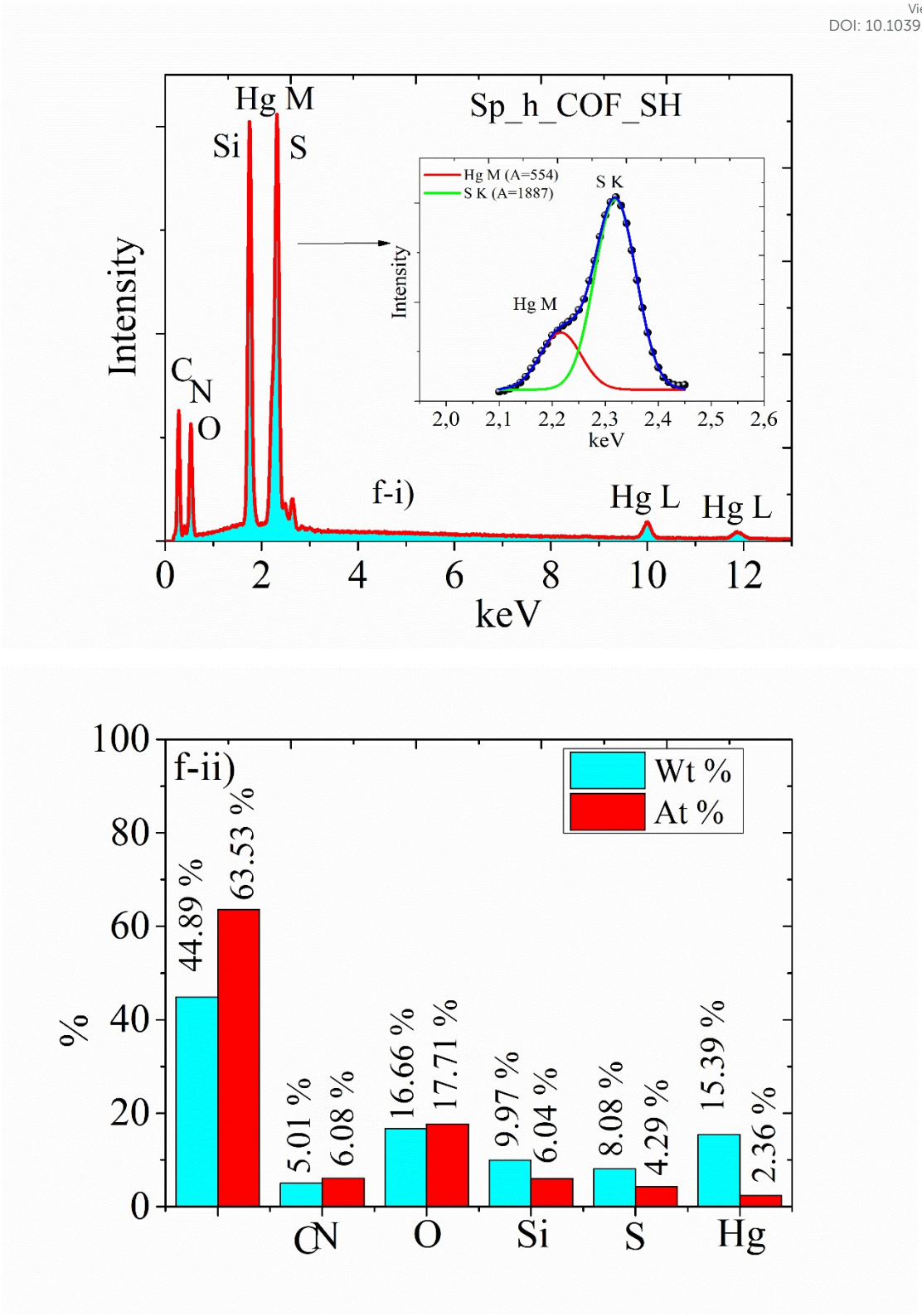

Figure 10. a) The fractions of Hg^{2+}, $HgOH^{+}$, $Hg(OH)_2$ and $Hg(OH)_3^-$ for pH levels from 0 to 14. Dynamic adsorption experiment for Sp_h_COF (b; blue: multivalent solution; cyan: divalent mercury solution), Sp_h_COF_SH (c; divalent mercury) and Sp_h_COF_SH (d; multivalent solution). e) Images of the three samples after the

View Article Online
DOI: 10.1039/D6MA00413J

experiment. f) EDS spectrum (i) and quantitative analysis graph (ii) for the Sp_h_COF_SH sample after the dynamic adsorption of mercury.

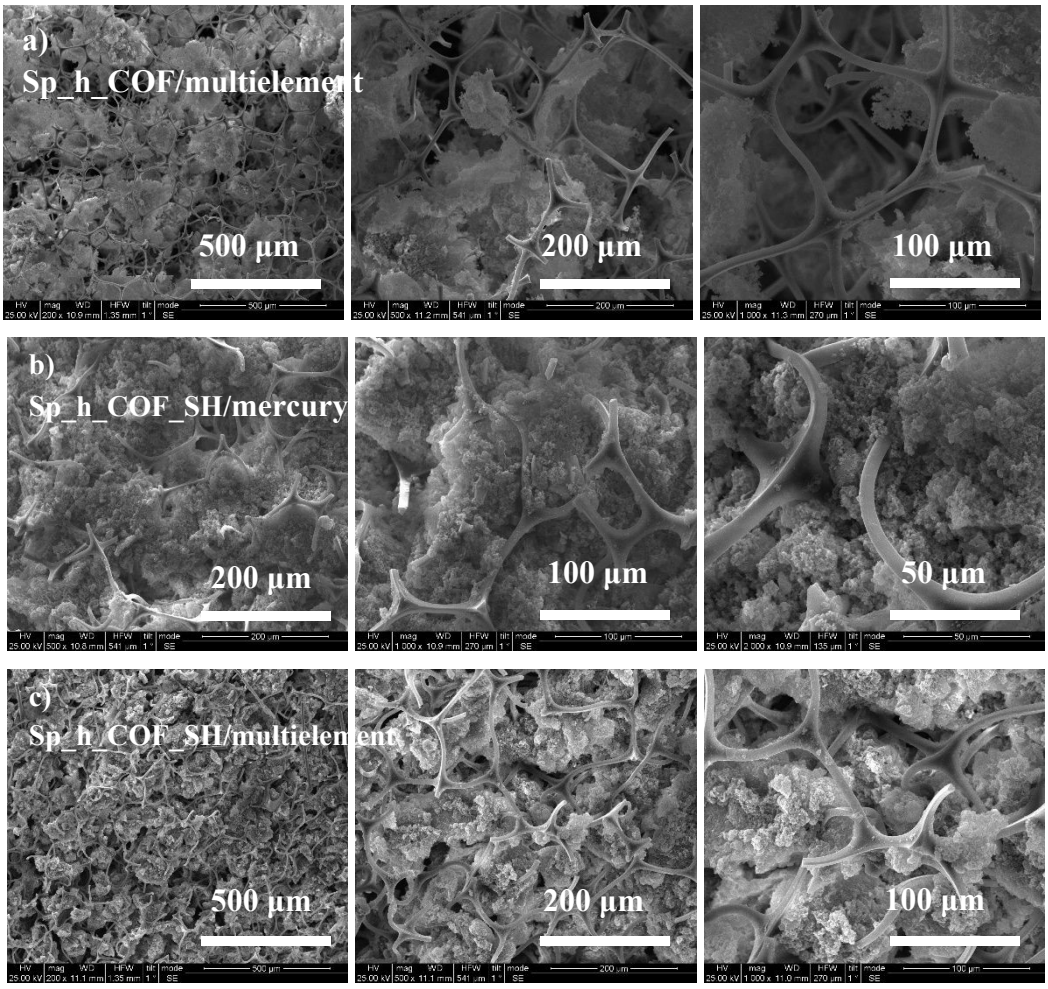

Figure 11. SEM images of the sponges after the heavy metal dynamic adsortion a) Sp_h_COF/multielement solution b) Sp_h_COF_SH/mercury solution c) Sp_h_COF_SH/multielement solution

Conclusions

In conclusion, we present the synthesis, characterization, stability evaluation, and application as dissolved oil and mercury adsorber of thiol functionalized imine COFs on commercial melamine sponges. The in-situ Schiff-base condensation of the precursors took place upon the hydrophobic sponges and the crucial thiol-ene coupling reaction of the COF were demonstrated through EDS and FTIR spectroscopy, while their structure and morphology were characterized by XRD and SEM during all the synthesis steps. The critical role of the thiol group for the efficiency of the material in water remediation was demonstrated through dynamic adsorption experiments, and a

View Article Online
DOI: 10.1039/D6MA00413J

quantitative analysis was performed using UV-Visible and ICP-OES techniques. The oil adsorption follows a first-order kinetic mechanism with different active sites, with a rapid exponential decay of capacity. The sponges present excellent removal efficiency of highly toxic metals such as mercury in dynamic adsorption experiments. The thiol-terminated COF exhibited an excellent removal efficiency of 77-99 % in 5 minutes interval measurements of dynamic flow of 10 and 100 ppm solutions. The selective adsorption of mercury is highlighted throughout multiple cycles in the presence of 27 competitive elements. By tailoring the coverage of the sponge with the COF, a material with a high cost of preparation, the system will find its way in real-life applications with respect to their efficiency and stability in consecutive experiments under dynamic conditions.

Acknowledgements. We acknowledge the support from the project ‘‘ATTP4 0359579” COF4SEA’’ (MIS 5217185) co-financed by the European Union and Greek National Funds through the Operational Program ATTIKA 2014-2020, under the call RESEARCH AND INNOVATION COOPERATIONS IN THE REGION OF ATTICA.

Supporting information. The S.I. is available free of charge via the internet. **Figure S1**: Diffuse reflectance spectra. **Figure S2**. COF powders with and without thiol were removed mechanically from the sponges and dispersed in water. **Figure S3**: Video and photo of the preparation of oil/water emulsion using high-share emulsifier. **Figure S4**: FTIR spectra. **Figure S5**: Image and video of the preparation of the emulsion. **Figure S6**: The reference emulsions and the corresponding calibration curve. **Figure S7**: Video of the first oil removal cycle using the thiol functionalized sponge. **Figure S8**: Oil adsorption curve of the pristine sponge. **Figure S9**: Bangham model graph. **Table S1** and **Table S2**: Quantitative EDS analysis data

Author contributions. P. B.: conceptualization, methodology, formal analysis, investigation, data curation, writing – original draft, writing –review and editing. N. T.: conceptualization, methodology, formal analysis, investigation, data curation, writing – original draft. M.-A. G.: methodology, investigation, data curation. T. L.: methodology, investigation, writing original draft, data curation. L.-A. T.: methodology, investigation, writing original draft, data curation. D.T.: visualization,

View Article Online
DOI: 10.1039/D6MA00413J

project administration. A.K: methodology, investigation. N.Z: methodology, investigation. E.S: methodology, investigation. T.S. supervision, project administration. E. A. P.: methodology, investigation, supervision. P. D.: conceptualization, methodology, formal analysis, investigation, writing-original draft, supervision, visualization, project administration.

Conflict of interest declaration. The authors declare that there is no conflict of interest.

References

1. United States Environmental Protection Agency, Understanding Oil Spills And Oil Spill Response, 540-K-99-007 OSWER 9200.5-104A PB2000-963401, December 1999.
2. K. Sharma, G. Shah, K. Singhal and V. Soni, Comprehensive insights into the impact of oil pollution on the environment, *Reg. Stud. Mar. Sci*., 2024, **74**, 103516.
3. Y. Feng, J. Yao, Design of Melamine Sponge-Based Three-Dimensional Porous Materials toward Applications, *Ind. Eng. Chem. Res*., 2018, **57**(22), 7322–7330.
4. J. Li, Y. Yang, W. Ma, G. Li, Q. Lu, Z. Lin, One-pot room-temperature synthesis of covalent organic framework-coated superhydrophobic sponges for highly efficient oil-water separation, *J. Hazard. Mater.,* 2021, **411**, 125190.
5. B. Dai, Y. Ding, C. Chen, L. Shen, D. L. Zhao, Y. Jiao, H. Lin, Y. Xu, Super-hydrophilic membranes fabricated by synergistic integration of covalent organic framework nanoflowers and hydrophilic layers for efficient oil-water separation, *Desalination,* 2024, **592**, 118095.
6. D. Cong, Q. Li, B. Zhao, L. Wang, W. Kan, B. Liu, F. Bu, Y. He, Fluorine-free self-hydrophobic covalent organic framework for unidirectional oil-water and emulsion separation, *Colloids Surf. A Physicochem. Eng. Asp.,* 2025, **725**, 137711.
7. W. Zhang, X. Zhai, T. Xiang, M. Zhou, D. Zang, Z. Gao, C. Wang, Superhydrophobic melamine sponge with excellent surface selectivity and fire retardancy for oil absorption, *J. Mater. Sci.,* 2017, **52:73**, 85.

8. Q. Sun, B. Aguila, J.A. Perman, T. Butts, F-S. Xiao, S. Ma, Integrating Superwettability within Covalent Organic Frameworks for Functional Coating, *Cell* 2018, **4**(7), 1726.
9. B. Fei-Baffoe, E. Badu, K. Miezah, L.N.A. Sackey, A. Sulemana, E. Ebo Y. Amuah, Contamination of groundwater by petroleum hydrocarbons, *Heliyon* 2024, **10**, e25924.
10. C. Morosini, E. Terzaghi, G. Raspa, E. Zanardini, S. Anelli, S. Armiraglio, E. Petranich, S. Covelli, A. Di Guardo, Mercury vertical and horizontal concentrations in agricultural soils of a historically contaminated site: Role of soil properties, chemical loading, and cultivated plant species in driving its mobility, *Environ. Pollut.* 2021, **285**, 117467.
11. S. V. Saghir and E. K. Goharshadi, Multifunctional MnO2 nanorods-modified wood sponge for water remediation: applications for heavy metal sorption and oil/water separation, *Wood Sci. Technol*., 2024, **58**, 2097–2113.
12. S.A. Ali, M.A.J. Mazumber, A new resin embedded with chelating motifs of biogenic methionine for the removal of Hg(II) at ppb levels, *J. Hazard. Mat.* 2018, **350**, 169-179.
13. J. Cao, Y. Wang, D. Wang, R. Sun, M. Guo, S. Feng, A Super-Amphiphilic 3D Silicone Sponge with High Porosity for the Efficient Adsorption of Various Pollutants, *Macromol. Rapid Commun*. 2021, **42**, 2000603.
14. H. Zhu, D. Chen, S. Yang, N. Li, Q. Xu, H. Li, L. Wang, J. He, J. Jiang and J. Lu, A versatile and cost-effective reduced graphene oxide-crosslinked polyurethane sponge for highly effective wastewater treatment, *RSC Adv*. 2016, **6**, 38350.
15. L. Wang, J. Li, Q. Jiang, L. Zhao, Water-soluble Fe_3O_4 nanoparticles with high solubility for removal of heavy-metal ions from wastewater, *Dalton Trans*. 2012, **41**, 4544-4551.
16. P. Bika, N. Ioannidis, P. Tsipas, S. Papagiannis, M-A. Gatou, E. A. Pavlatou, A. G. Karydas, T. Stergiopoulos, P. Dallas, Detection and Selective Sorption of Copper Ions by a COF-Modified Melamine Sponge, *ACS Omega* 2025, **10**, 21755−21766.
17. P. Bika, N. Ioannidis, M-A. Gatou, Y. Sanakis, P. Dallas. Copper Coordination and the Induced Morphological Changes in Covalent Organic Frameworks, *Langmuir* 2022, **38**, 3082−3089,

18. P. Das, S.K. Mandal, In-depth experimental and computational investigations for remarkable gas/vapor sorption, selectivity, and affinity by a porous nitrogen-rich covalent organic framework, *Chem. Mater*., 2019, **31**, 1584-1596,
19. C. Arqueros, L. Welte, C. Montoro, F. Zamora, Imine-based covalent organic framework gels for efficient removal of Fe^{2+} from contaminated water, *J. Mater. Chem. A*, 2024, **12**, 20121-20128.
20. T. Chen, W-N. Jiao, W-D. Zhu, H. Wang, S. Huang, X-C. Lin, J. Liu, H-S. Xu, C-Y. Su, Designed Synthesis of Imine-Linked 2D Covalent Organic Frameworks with Enhanced Stability and Functionality, *Chem. Mater*. 2024, **36(15)**, 7362–7369.
21. Q. Sun, B. Aguila, J. Perman, L.D. Earl, C.W. Abney, Y. Cheng, H. Wei, N. Nguyen, L. Wojtas, S. Ma, Postsynthetically Modified Covalent Organic Frameworks for Efficient and Effective Mercury Removal, *J. Am. Chem. Soc*. 2017, **139**, 2786−2793,
22. P. Bika, N. Todorova, M-A. Gatou, M. Pissas, E. Devlin, E. Sakellis, N. Boukos, N. Lagopati, T. Lymperopoulou, L-A. Tsakanika, E.A. Pavlatou, V.K. Tzitzios, P. Dallas, Magnetically controllable sponges for crude oil, mercury, and arsenic removal, *Environ. Sci. Nano* 2026, **13**, 280-295.
23. M. H. Tai, J. Juay, D. D. Sun, J. O. Leckie, Carbon–silica composite nanofiber membrane for high flux separation of water-in-oil emulsion – Performance study and fouling mechanism, *Sep. Purif. Technol*., 2015, **156**, 952.
24. H. Gao, P. Sun, Y. Zhang, X. Zeng, D. Wang, Y. Zhang, W. Wang, J. Wu. Two-step hydrophobic fabrication of melamine sponge for oil absorption and oil/water separation, *Surf. Coat. Technol*., 2018, **339**, 147–154.
25. X. Jiang, X. Tang, L. Tang, B. Zhang, H. Mao, Synthesis and formation mechanism of amorphous silica particles via sol–gel process with tetraethylorthosilicate, *Ceram. Int.,* 2019, **45**, 7673–7680
26. G.O. Kayan, I. Akin, Ti_3SiC_2 MAX phase: Sol–gel processing, characterization, and sinterability, *J. Am. Ceram. Soc*,. 2026, **109(1)**, e70341
27. X. Li, C. Zhang, S. Cai, X. Lei, V. Altoe, F. Hong, J.J. Urban, J. Ciston, E.M. Chan, Y. Liu, Facile transformation of imine covalent organic frameworks into ultrastable crystalline porous aromatic frameworks, *Nat. Commun*., 2018, **9**, 2998,

28. C. Miao, X. Xun, L.J. Dodd, S. Niu, H. Wang, P. Yan, X-C. Wang, J. Li, X. Wu, T. Hassell, Z-J. Quan, Inverse Vulcanization with SiO_2-Embedded Elemental Sulfur for Superhydrophobic, Anticorrosion, and Antibacterial Coatings, *ACS Appl. Polym. Mater*., 2022, **4(7)**, 4901–4911.
29. P. Bika, V. Tzitzios, I. Sakellis, S. Orfanoudakis, N. Boukos, S.M. Alhassan, P. Tsipas, V. Psycharis, T. Stergiopoulos, P. Dallas, Electron transfer and energy exchange between a covalent organic framework and $CuFeS_2$ nanoparticles, *J. Mater. Chem.C*., 2024, **12**, 10475-10486.
30. E. Dautzenberg, M. Lam, T. Nikolaeva, W.M.J. Franssen, B. van Lagen, I.P.A.M. Gerrits-Benneheij, N. Kosinov, G. Li, L.C.P.M. de Smet, Tuning UV Absorption in Imine-Linked Covalent Organic Frameworks via Methylation, *J. Phys. Chem. C.,* 2022, **126**(50), 21338–21347,
31. H. Li, T. Liang, X. Lai, X. Su, L. Zhang, X. Zeng, Vapor-liquid interfacial reaction to fabricate superhydrophilic and underwater superoleophobic thiol-ene/silica hybrid decorated fabric for oil/water separation, *Appl. Surf. Sci*., 2018, **427**, 92-101.
32. L.B. Poole, The basics of thiols and cysteines in redox biology and chemistry, *Free Radic. Biol. Med*., 2015, **80**, 148-157.
33. P. Gao, K. Tang, R. Lou, X. Liu, R. Wei, N. Li, B. Tang, Covalent Organic Framework-Based Spherical Nucleic Acid Probe with a Bonding Defect-Amplified Modification Strategy, *Anal. Chem*., 2021, **93**(35), 12096–12102.
34. Y. Pan, X. Zhang, W. He, L Zheng, X. Han, Dha Tab-COF filled PEBAX mixed matrix membranes for effective CO_2/CH_4 separation, *Chin. J. Chem. Eng.*, 2025, **77**, 123-134.
35. Z. Kuodis, I. Matulaitienė, M. Špandyreva, L. Labanauskas, S. Stončius, O. Eicher-Lorka, R. Sadzevičienė, G. Niaura, Reflection Absorption Infrared Spectroscopy Characterization of SAM Formation from 8-Mercapto-N-(phenethyl)octanamide Thiols with Phe Ring and Amide Groups, *Molecules* 2020, **25**(23), 5633.
36. Z.B. Khorshid, M.M. Doroodmand, S. Abdollahi. UV–Vis. spectrophotometric method for oil and grease determination in water, soil and different mediates based on emulsion. *Microchem. J*. 2021, **60**, 105620
37. Y. Zhang, G.D. Bland, J. Yan, A. Avellan, J. Xu, Z. Wang, T.P. Hoelen, F. Lopez-Linares, E.S. Hatakeyama, K. Matyjaszewski, R.D Tilton, G.V. Lowry,

Amphiphilic Thiol Polymer Nanogel Removes Environmentally Relevant Mercury Species from Both Produced Water and Hydrocarbons, *Environ. Sci. Technol*., 2021, **55**, 1231-1241.

38. J. Yan, J. Cao, L. Xue, S. Feng, H. Zhang, D. Wang, Thiol Oxidative Coupling Synthesis of Silicone Foams for Oil/Water Separation, *ACS Appl. Polym. Mater*. 2020, **2**(4), 1634–1643.
39. F-C. Wu, R-L. Tseng, R-S. Juang, Characteristics of Elovich equation used for the analysis of adsorption kinetics in dye-chitosan systems, *Chem. Eng. J*., 2009, **150**, 366-373.
40. A. Kayan, M.O. Arican, Y. Boz, U. Ay, S.K. Bozdas. Novel tyrosine-containing inorganic–organic hybrid adsorbent in removal of heavy metal ions *J.Environ.Chem.Eng*. 2014, **2**, 935-942
41. Z. Yang, S.Fang, M. Duan, Y. Xiong, X. Wang, Chemisorption mechanism of crude oil on soil surface, *J. Hazard. Mater.* 2020, **386**, 121991.
42. R. Gurav, S. K. Bhatia, T-R. Choi, Y-K. Choi, H. J. Kim, H-S. Song, S. L. Park, H. S. Lee, S. M. Lee, K.-Y. Choi, Y-H. Yang, Adsorptive removal of crude petroleum oil from water using floating pinewood biochar decorated with coconut oil-derived fatty acids, *Sci. Total Environ*., 2021, **781**, 146636.
43. A.K. Nayak, A. Pal, Development and validation of an adsorption kinetic model at solid-liquid interface using normalized Gudermannian function, *J. Mol.Liq*., 2019, **276**, 67-77.
44. X. Li, Z. Jia, H-W. Tan, Yu Yang, Li-An Hou, Enhanced simultaneous adsorption and detection of mercury (II) using functionalized metal − organic framework with defect structures, *Sep. Purif. Technol*., 2025, **354**(7), 129110.
45. Y. Wang, S. Li, X. Wu, J. Zhang, J. Feng, M. Li, S. Zong, W. Yan, Nitrogen-Based conjugated microporous polymers for efficient Hg(Ⅱ) removal from Water: Performance and mechanism, *Chem. Eng. J.,* 2023, **471**, 144659.
46. F-S. Zhang, J.O. Nriagu, H. Itoh, Mercury removal from water using activated carbons derived from organic sewage sludge, *Water Res.,* 2005, **39**(2-3), 389-395.
47. L-Y. Chai, Q-W. Wang, Y-Y. Wang, Q-Z. Li, Z-H. Yang, Y-D. Shu, Thermodynamic study on reaction path of Hg(Ⅱ) with S(Ⅱ) in solution, *J. Cent. South Univ. Technol*., 2010, **17**, 289−294.

View Article Online
DOI: 10.1039/D6MA00413J

48. B. Shi, H. Li, X.Fu, C. Zhao, A.H. Wang, W. Tan, Y. Rao, M. Li, S. Komarneni, H. Yang, Insight into the key role of imine groups in polyaniline for adsorbing heavy metal ions: Density functional theory and experimental study, *Sep. Purif. Technol.,* 2024, **335**, 125866.
49. T. Velempini, K. Pillay, Sulphur functionalized materials for Hg(II) adsorption: A review, *J. Environ. Chem. Eng.,* 2019, **7(5)**, 103350.

View Article Online
DOI: 10.1039/D6MA00413J

Data for this article are either included in the manuscript or are available upon request by the corresponding authors